Systematics of isomeric configurations in $N = 77$ odd-Z isotones near the proton drip line

M. N. Tantawy,* C. R. Bingham,[1,2] K. P. Rykaczewski,[2] J. C. Batchelder,[3] W. Królas,[4,5,6] M. Danchev,[1] D. Fong,[4] T. N. Ginter,[7] C. J. Gross,[2] R. Grzywacz,[1,2] K. Hagino,[8] J. H. Hamilton,[4] D. J. Hartley,[1,†] M. Karny,[9] K. Li,[4] C. Mazzocchi,[1] A. Piechaczek,[10] A. V. Ramayya,[4] K. Rykaczewski,[11] D. Shapira,[2] A. Stolz,[7] J. A. Winger,[12] C.-H. Yu,[2] and E. F. Zganjar[10]

[1]*Department of Physics and Astronomy, University of Tennessee, Knoxville, Tennessee 37996, USA*

[2]*Physics Division, Oak Ridge National Laboratory, Oak Ridge, Tennessee 37831, USA*

[3]*UNIRIB, Oak Ridge Associated Universities, Oak Ridge, Tennessee 37831, USA*

[4]*Joint Institute for Heavy Ion Research, Oak Ridge, Tennessee 37831, USA*

[5]*Department of Physics and Astronomy, Vanderbilt University, Nashville, Tennessee 37235, USA*

[6]*Institute of Nuclear Physics, Polish Academy of Sciences, PL-31-342 Kraków, Poland*

[7]*National Superconducting Cyclotron Laboratory, Michigan State University, East Lansing, Michigan 48824, USA*

[8]*Department of Physics, Tohoku University, Sendai, 980-8578 Japan*

[9]*Institute of Experimental Physics, Warsaw University, Warsaw, PL-00681, Poland*

[10]*Department of Physics and Astronomy, Louisiana State University, Baton Rouge, Louisiana 70803, USA*

[11]*G. W. School of Mechanical Engineering, Georgia Institute of Technology, Georgia 30332, USA*

[12]*Department of Physics and Astronomy, Mississippi State University, Mississippi State, Mississippi 39762, USA*

(Received 16 September 2005; published 22 February 2006)

The systematics of the $\pi h_{11/2} \otimes \nu h_{11/2}$ and $\pi h_{11/2} \otimes \nu s_{1/2}$ isomeric configurations was studied for the odd-Z $N = 77$ isotones near the proton drip line. The isomeric decays in ^{140}Eu, ^{142}Tb, ^{144}Ho, and ^{146}Tm were measured by means of x-ray, γ-ray, and charged particle spectroscopy at the Recoil Mass Spectrometer at the Holifield Radioactive Ion Beam Facility (ORNL). The spin and parity of $I^\pi = 8^+$ and 5^- were deduced for the isomers in ^{140}Eu and ^{142}Tb. New decay schemes were established, and the half-lives of the 8^+ isomers were measured to be 302(4) ns for ^{140m2}Eu and 25(1) μs for ^{142m2}Tb. No evidence for the expected 1^+ ground-state was found in the ^{144}Ho decay data. The proton-emission from ^{146}Tm was restudied. Five proton transitions were assigned to two proton-emitting states. The half-lives of 198(3) ms and 68(3) ms and the spin and parity values of $I^\pi = 10^+$ and 5^- were established for ^{146m}Tm and ^{146gs}Tm, respectively. For the first time for an odd-odd nucleus, the interpretation of the observed decay properties and structure of the proton-emitting states was made by accounting for deformation and proton and neutron coupling to the core excitations. A complex wave-function structure was obtained, with dominating components of $\pi h_{11/2} \otimes \nu h_{11/2}$ for the 10^+ isomer and $\pi h_{11/2} \otimes \nu s_{1/2}$ for the 5^- ground state.

DOI: 10.1103/PhysRevC.73.024316 PACS number(s): 23.20.Lv, 21.10.Tg, 23.50.+z, 27.60.+j

I. INTRODUCTION

The presence of excited isomeric states in atomic nuclei is a sign of γ-decay hindrance. The isomerism of a state is caused by the absence of energetically available states with large decay probability. Isomeric decays sometimes require a major rearrangement of nucleons, and in extreme cases it can lead to β or particle decay. The isomers are thus signatures of major structure changes within the nucleus. Their presence enables a detailed experimental study since the stopover in the prompt decay path allows the use of very selective time-delayed correlation/tagging techniques. Isomeric states in the $N = 77$ region are a result of the high-j states that involve the $h_{11/2}$ intruding proton orbitals and their associated high-multipolarity decays. In addition, the $h_{11/2}$ proton orbitals tend to favor collective prolate deformed shapes with $\gamma = 0°$; the neutron configurations, being in the upper part of the $h_{11/2}$ shell, tend to favor collective oblate nuclear shapes with $\gamma = -60°$. The prolate and the oblate potential-energy minima are predicted to have similar energies [1].

For the odd-odd $N = 77$ isotone ^{146}Tm, two proton-radioactive states are known and both exhibit fine structures in the proton-emission spectra [2–4]. However, in the previous work, there was an ambiguity in the spin and configuration assignment. Even the possibility of a third proton-emitting state was considered [2]. We have restudied the decay of ^{146}Tm, establishing the half-life of the 1.016-MeV proton transition and determining its origin.

The interpretation of the structures of proton-emitting nuclei often suffers from the lack of data on nuclei next to the proton drip line. To better understand the systematic trends of the proton-neutron states around the proton drip line, we studied the $N = 77$ even-mass isotones next to ^{146}Tm, namely ^{144}Ho, ^{142}Tb, and ^{140}Eu (see Fig. 1 for previous information from the literature [1,2,5–16] and this work).

II. EXPERIMENTAL SETUP

The ^{140}Eu, ^{142}Tb, and ^{144}Ho nuclei were produced at the Holifield Radioactive Ion Beam Facility (HRIBF) at Oak Ridge in fusion-evaporation reactions between ^{54}Fe projectiles,

*Part of M. N. Tantawy's Ph.D. dissertation, with ^{146}Tm data analyzed by J. C. Batchelder and M. N. Tantawy.

†Present address: Department of Physics, United States Naval Academy, Annapolis, Maryland 21402, USA.

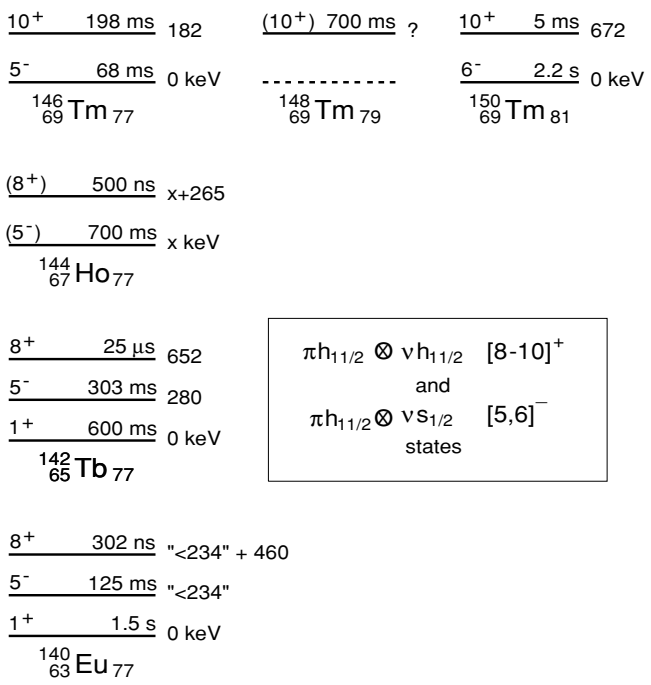

FIG. 1. Systematics of the $\pi h_{11/2} \otimes \nu h_{11/2}$ and the $\pi h_{11/2} \otimes \nu s_{1/2}$ states in the $N = 77$ odd-Z isotones and $Z = 69$ odd-N thulium isotopes around the proton drip line. The spin and parity assignments are from this work and from the literature [1,2,5–16].

at 315, 250 and 225 MeV, respectively, and a 98.7% enriched, 1-mg/cm^2 ^{92}Mo target. Recoiling ions were separated according to their mass-to-charge (A/Q) ratio by the Recoil Mass Spectrometer (RMS) [17]. The time of flight from the target to the focal plane of the RMS was about 2.2, 2.5, and 2.8 μs for ^{140}Eu, ^{142}Tb, and ^{144}Ho recoils, respectively. The recoils passed through a position-sensitive microchannel plate (MCP) detector [18] located at the final focal plane of the RMS. The MCP provided recoil implantation time reference and position signals. The detailed experimental setup used in the study of ^{140}Eu can be found in Ref. [19]. In the case of ^{142}Tb and ^{144}Ho, the recoils were implanted in an aluminized Mylar tape in the moving tape collector [20] located at the final focus of the RMS. A degrader copper foil (2.3 mg/cm^2) was placed in front of the implantation point of the tape. This foil slowed the 60-MeV ^{142}Tb ions to about 10 MeV, resulting in an implantation depth of about 3.3 μm. Electrons with energies below 20 keV emitted at this depth were stopped in the tape, and measured energies of 85-keV electrons were shifted down by about 3 keV. The moving tape collector was surrounded by a low-energy photon detector (LOAX) with a thin Be window, two segmented Ge clover detectors, and a high-resolution 180-mm^2 Si(Li) conversion electron spectrometer [20] called the Bellows Electron Spectrometer for the Cards Array (BESCA) (see Fig. 2). All four detectors were mounted on the Clover ARray for Decay Studies (CARDS).

Efficiency curves for the detectors were determined by use of standard sources. The summed efficiency of the two clover detectors was measured to be 13.6% at 121 keV and 2.7% at 1408 keV by a ^{152}Eu source. The maximum efficiency of the LOAX detector was about 6.9% at 121 keV.

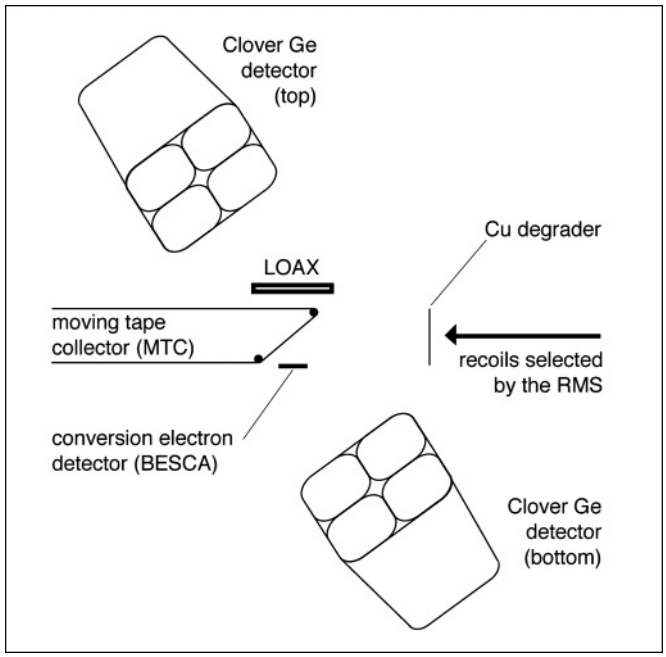

FIG. 2. Schematic diagram of the setup used in the study of odd-Z $N = 77$ isotones ^{142}Tb and ^{144}Ho at the HRIBF. The setup was placed at the final focus of the RMS.

The effective measurement time of ^{142}Tb with the BESCA was 8 h with an average ^{54}Fe beam current of 20 pnA. This was sufficient to determine the multipolarities of most of the transitions deexciting the isomeric states in ^{142}Tb along with the spins and parities of all populated states. No electron data were collected for $A = 140$ and $A = 144$ nuclei.

The decay of the proton radioactive $N = 77$ isotone ^{146}Tm was restudied at the RMS. The nuclei of interest were produced in the fusion-evaporation reaction between a 297-MeV ^{58}Ni beam and a 0.91-mg/cm^2 ^{92}Mo target. The reaction products were separated by the RMS and implanted at the final focal plane into a 65-μm-thick double-sided Si strip detector (DSSD) [21]. Before implantation into the DSSD, the recoils passed through two MCP detectors (see Fig. 3). The larger MCP was used to observe the mass dispersion of the recoils and

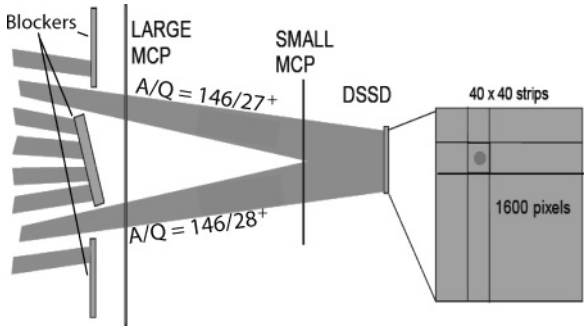

FIG. 3. Schematic diagram of the recoils passing through the two MCPs and the two-slit three-blocker system to be finally implanted in the DSSD at the final focus of the RMS in the ^{146}Tm proton-emitter study. The large MCP was used for A/Q identification of the recoils. The small MCP was used as an additional timing reference.

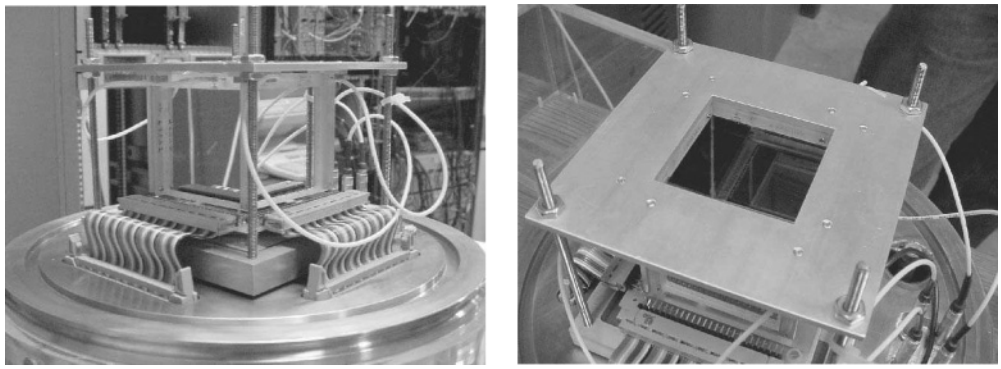

FIG. 4. Photographs of the detection setup used during the ^{146}Tm experiment. The 65-μm-thick DSSD was surrounded by four 700-μm-thick Si detectors mounted in a box geometry. The left-hand picture shows a side view of the setup while the right-hand picture shows an angled top view. Below the DSSD is a Si(Li) detector, 45 mm × 45 mm, with an active measuring thickness of 3.9 mm.

to record the implantation time, while the smaller MCP, located closer to the DSSD, was used to give redundant information of implantation signal timing. Once the proper A/Q was identified, a two-slit three-blocker system was used in front of the MCPs to select the desired A/Q, 146/27 and 146/28, ions to pass.

The DSSD was surrounded by four 700-μm-thick silicon detectors forming a Si box (see Fig. 4). The Si box signals were used to veto escape protons and α particles that release only part of their energy in the DSSD and therefore add to the background. In Fig. 5 the effect of such background reduction is shown. A Si(Li) detector with an active measuring thickness of 3.9 mm was placed behind the DSSD for further vetoing of any particles escaping from the DSSD. The resolution of the DSSD detector for 5.5-MeV α particles from a ^{241}Am source was about 26 keV. The measurement lasted 96 h with an average ^{58}Ni beam current of about 20 pnA. In this experiment, the rate of recoils detected in the small MCP was about 1.2 kHz.

The signals from all RMS detectors in all three experiments were processed by 40-MHz digital gamma finder modules manufactured by X-Ray Instrumentation Associates [22].

III. RESULTS

A. ^{140}Eu

The β decay of ^{140}Eu^{gs} was first reported by Westgard [23], and a decay scheme was constructed by Beraud *et al.* [24]. Firestone *et al.* [1] investigated the decay of ^{140}Eu further and presented a more comprehensive picture of the decay. In Ref. [1], a metastable state, ^{140m1}Eu with $T_{1/2} = 125$ ms, was also reported.

Examination of the two-dimensional γ-ray energy versus time difference between the recoil implantation and the γ-ray detection data from our experiment revealed a subset of observed γ rays with a short decay time. By gating on the first microsecond of the two-dimensional spectrum and subtracting the spectrum gated on the second microsecond, we obtained a spectrum of γ rays correlated with the decay of the recoils with submicrosecond half-lives; see Fig. 6(a). The properties of the measured γ-ray transitions are listed in Table I. We examined the coincidence relations for γ rays from this short-lived isomer by generating an E_γ–E_γ coincidence matrix. As an example, Fig. 6(b) shows the γ-ray spectrum obtained in coincidence with the 170.4-keV γ line. This coincidence

TABLE I. Decay properties of the $I^\pi = 8^+$ isomer in ^{140}Eu. The energies, intensities, conversion coefficients, and multipolarities are listed for the observed γ transitions.

E_γ (keV)	Rel. I_γ (%)	Measured α_K, $\alpha_{\text{total}}^{\text{a}}$	Multipolarity (literature) [6]	Adopted multipolarity (this work)	I_{total} (%)
33.0(10)	6(3)	$\alpha_T = 7.1$		$(M1)$	24(12)
37.1(3)	100(9)	$\alpha_T = 0.65(28)$	$M1$	$E1$	83(8)
98.1(3)	26(3)	$\alpha_K = 0.3(1)$	$E1$	$E1$	17(2)
104.5(3)	9(2)	$1.6 < \alpha_T < 2.1$	$E1$	$(M1/E2)$	13(3)
137.5(3)	15(3)	$0.75 < \alpha_T < 0.78$	$E1$	$(M1/E2)$	13(3)
170.4(3)	53(7)	$\alpha_K = 0.4(1)$	$M1$	$M1/E2$	37(6)
190.8(3)	16(4)	$\alpha_T = 0.21(7)$	$M1$	$M1/E2$	10(2)
252.0(3)	50(7)	$\alpha_T = 0.11(5)$	$(E1)$	$M1/E2$	28(4)
284.8(3)	38(6)	$\alpha_K = 0.08(3)$	$M1/E2$	$M1/E2$	21(3)
361.5(3)	14(4)	$\alpha_T = 0.03$	$E2$	$E2$	7(2)
389.2(3)	7(3)	$\alpha_T = 0.027$	$(M2)$	$(E2)$	4(2)
422.5(3)	59(10)	$\alpha_T = 0.02$	$(M2)$	$E2$	30(5)

[a]Values of α with uncertainties are our measured values while the others are calculated values.

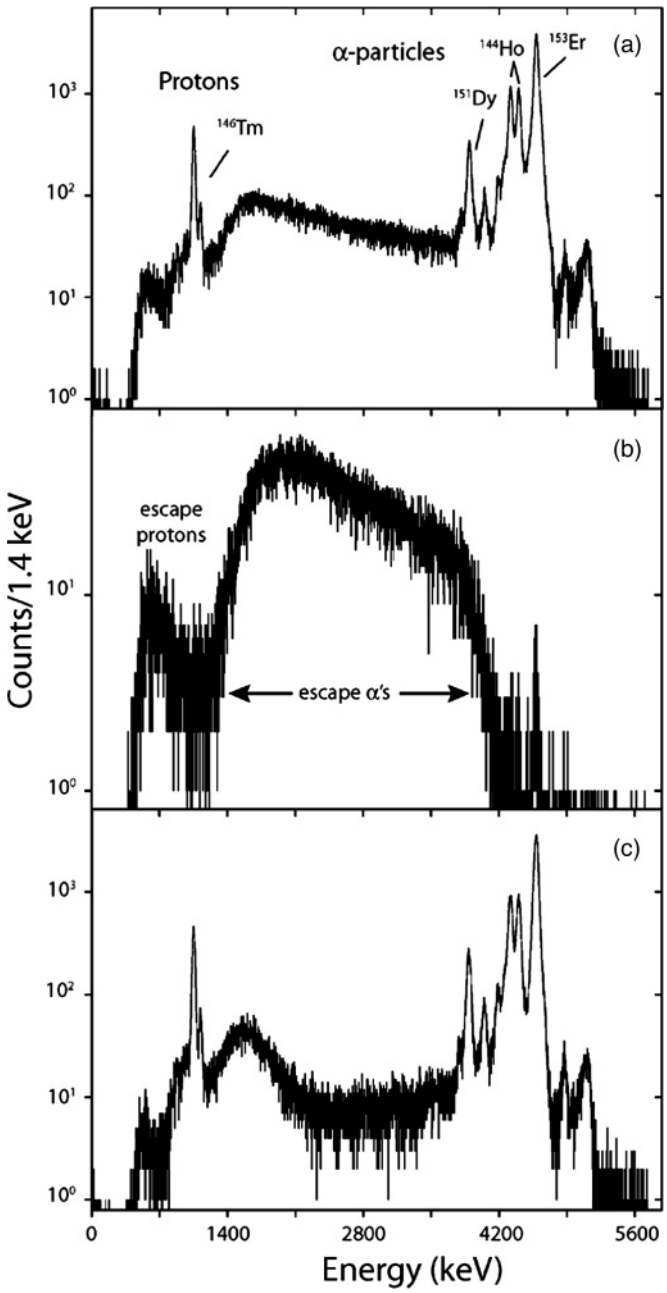

FIG. 5. (a) Energy spectrum of protons and α particles from the DSSD with no veto applied. (b) Energy spectrum of the particles detected in the DSSD in coincidence with any of the Si box detectors. (c) Energy spectrum of protons and α particles from the DSSD in anticoincidence with the Si box detectors and the SiLi detector. A rigid-mass gate was also applied here and a condition that the front and back energy spectra of the DSSD be in agreement with each other within 2%.

(and others) revealed Eu x-ray energies $K_\alpha \approx 41$ keV and $K_\beta \approx 47$ keV, thus establishing the cascade as the decay of an isomeric state in ^{140}Eu [5]. The half-life, $T_{1/2} = 302(4)$ ns, of this isomer, ^{140m2}Eu, was deduced from the decay pattern of the summed 98.1-, 170.4-, 252.0-, and 422.5-keV γ rays; see Fig. 7. Our $T_{1/2}$ value agrees well with two independent studies published recently [6,7].

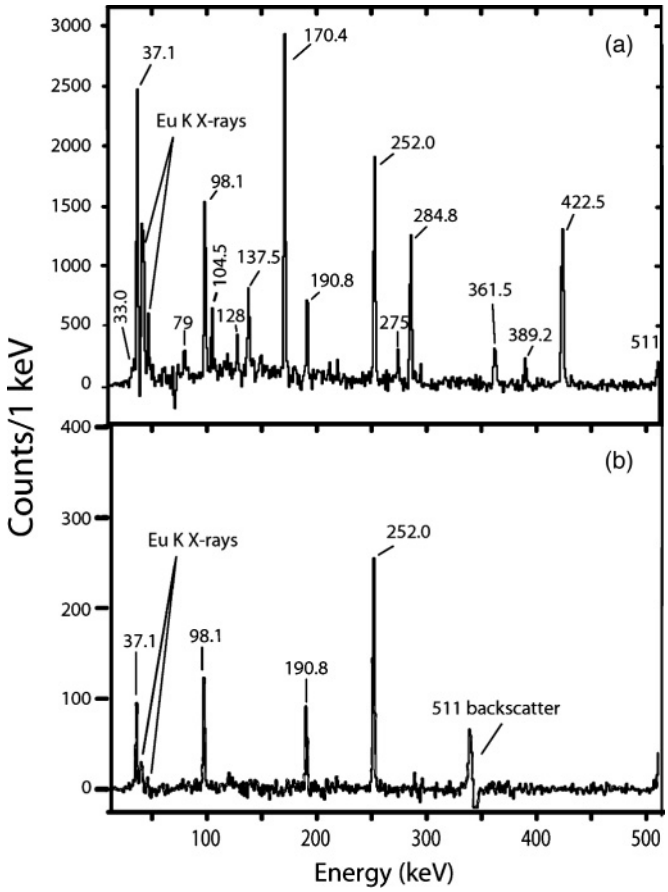

FIG. 6. (a) Spectrum of γ rays collected within 1 μs of an implant minus γ rays collected between 1 and 2 μs during the $A = 140$ measurement. The 79-, 128-, and 275-keV lines shown in the figure are long-lived impurities and are not in coincidence with the Eu x-rays. (b) Spectrum of γ rays in coincidence with the 170.4-keV line in the decay of ^{140m2}Eu.

In addition, we obtained experimental verification of relative position of two isomers, ^{140m2}Eu and ^{140m1}Eu, with the 302-ns level above the 125-ms activity; see Fig. 8. Figure 9 shows the 175- and the 185-keV transitions, known to deexcite the 125-ms level [1], in the γ-ray spectrum following the decay of the 302-ns activity within 200 ms. It confirms independently the sequence of isomeric levels given in Refs. [6,7]. Other lines appearing in Fig. 9, such as the 39-keV Sm K x-ray line and others are believed to be the result of random accidental correlations. Sm K x-rays represent the strongest lines in the singles γ-ray spectrum. The excitation energy of the ^{140m1}Eu isomeric state deexciting to the 1^+ ground state by means of the 175- and 185-keV transitions ($T_{1/2} = 125$ ms) has been postulated to be <234 keV with the spin and parity of $I^\pi = 5^-$ [1]. The energy limits for the nonobserved transitions deexciting the 125-ms $I^\pi = 5^-$ isomer, ^{140m1}Eu, of "<59" and "<49" keV, were suggested in Ref. [1]. The <59 and <49-keV γ rays are likely to be strongly L-converted transitions. A low-energy peak appears at 59 keV in Fig. 9. Its appearance does not allow a conclusion that it is real since its intensity error is larger than the total number of counts in that peak. For the 175- and 185-keV lines, however, the number of counts are

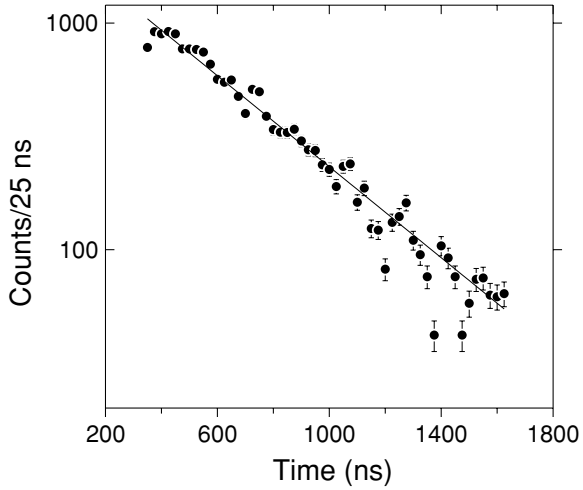

FIG. 7. Decay pattern of ^{140m2}Eu, $T_{1/2} = 302(4)$ ns, from the sum of 98.1-, 170.4-, 252.0-, and 422.5-keV γ lines after the appropriate background is subtracted. "Time" refers to the time difference between the implant signal and the recorded γ ray.

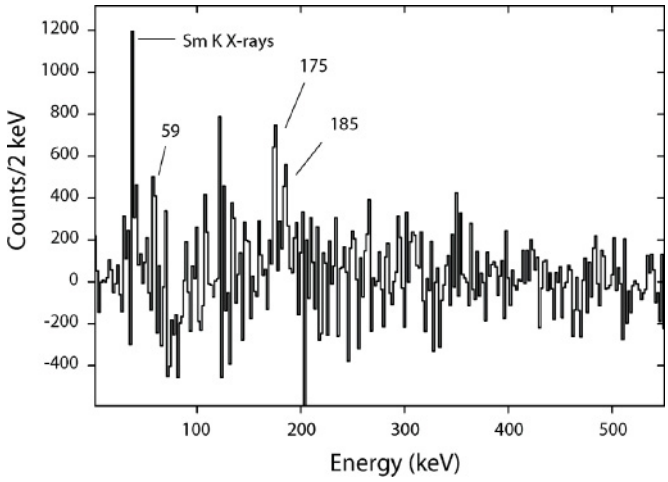

FIG. 9. γ rays following the decay of the 302-ns isomer (^{140m2}Eu) within the first 200 ms, less those from the 200–400 ms time window after the isomeric decay. The presence of the 175- and 185-keV lines indicates that the 302-ns ^{140m2}Eu isomeric decay feeds the 125-ms ^{140m1}Eu level. All other lines are believed to be the result of random accidental correlation.

1300(510) and 1050(440), respectively, which indicates that those lines are correlated with the transitions from the 302-ns isomeric level.

Using our results on ^{140m2}Eu and other available data on ^{140}Eu, we constructed a level scheme involving two isomeric states and the intermediate levels populated in their decay (see Fig. 8). The level scheme and the spin and parity assignments given in Fig. 8 are based on the coincidence relations and deduced multipolarities. By gating on the 252-keV line in our γ-γ matrix, we found $\alpha_K = 0.4(1)$ for the 170.4-keV γ ray by comparing the intensities of Eu K x-rays with the 170.4-keV photons. This is consistent with a parity-conserving $M1(E2)$ transition. It is consistent with the spin assignment of 5^- for ^{140m1}Eu [1,6,7] and the $I^\pi = 6^-$ found in Ref. [7] for the $X + 170.4$ keV level. The level at $X + 361.5$ keV was found to have $I^\pi = 7^-$ in Ref. [7] and to decay by means of the $E2$ 361.5-keV transition to the 5^- isomer. The calculated $\alpha_{\text{total}}(361.5, E2) = 0.03$. By comparing the total intensity of the 190.8-keV line with the difference of the total intensity between the 98.1- and the 361.5-keV lines, we determined $\alpha_{\text{total}}(190.8) = 0.21(7)$, which is consistent with a mixed $M1 + E2$ character. Finally, gating on the 361.5-keV line, we measured $\alpha_K = 0.3(1)$ for the 98.1-keV line, which is consistent with an $E1$ transition (see Table I). This $E1$ assignment for the 98.1-keV line defines the spin and parity of ^{140m2}Eu as 8^+. This assignment agrees with Ref. [6], but differs from the $I^\pi = 9^+$ adopted in Ref. [7].

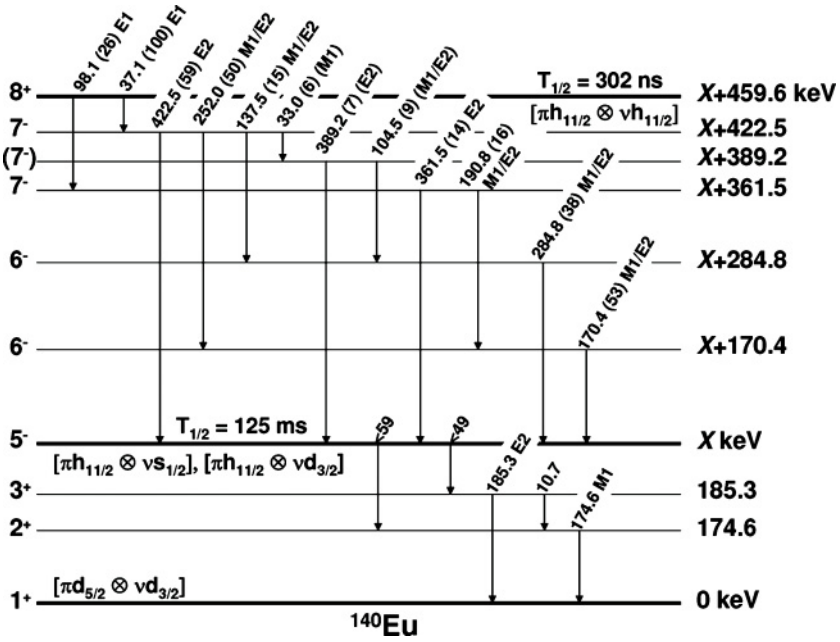

FIG. 8. Proposed ^{140}Eu level scheme from this work. The 125-ms, $I^\pi = 5^-$, isomer in the decay scheme was taken from Ref. [1] and was not directly studied in this work. The energy of this isomer, X, was reported in Ref. [1] to be <234 keV.

Besides the transitions showing the decay pattern corresponding to a 302-ns half-life, no other half-life component was observed for the γ lines deexciting the ^{140m2}Eu isomer. This indicates that the multipolarity of these transitions is lower than 3. The multipolarity $E3$ or $M3$ would make the half-lives of the parent states in the millisecond (or longer) range or reduce the γ intensity of the considered transition competing with lower multipolarity ones to the nondetectable level.

The decay of the $X + 422.5$ keV level populated by the single isomeric transition at 37.1 keV is followed by the transitions of 33.0, 104.5, 137.5, 170.4, 252.0, 284.8, 389.2, and 422.5 keV. For multipolarity <3, the total intensity of these transitions are too small to account for our observed intensity for the 37.1-keV transition for any multipolarity other than $E1(\alpha_{\text{total}} = 0.7)$ as compared with $\alpha_{\text{total}}(M1) = 5$ and $\alpha_{\text{total}}(E2) = 139$. Our finding disagrees with the relative intensity of the 37.1-keV line and the assignment of $M1$ multipolarity proposed in Ref. [6]. The 37.1-keV $E1$ line defines the spin and parity of 7^- for the $X + 422.5$ keV level. As a consequence, we assign only negative parity to the levels between the two ^{140}Eu isomers, in contrast to Ref. [6] and in agreement with Ref. [7]. The energy threshold for detecting γ rays in our experiment was lower in comparison with that of Ref. [6], and even allowed us to detect the 33.0-keV transition. The line at 33.0 keV was expected but not directly observed in Ref. [6]. The higher-energy threshold might be responsible for an artificial reduction of the 37.1-keV γ-ray intensity observed in Ref. [6].

The total conversion coefficient of 0.11(5) deduced for the 252.0-keV line, which we obtained by comparing its γ-ray intensity with that of the 170.4- and 190.8-keV lines, agrees with $M1 + E2$ character for this transition between the $X + 422.5$ and the $X + 170.4$ keV levels. Thus we assign $I^\pi = 7^-$ to the $X + 422.5$ keV level, as shown in Fig. 8. The $E2$ multipolarity can be assigned to the 422.5-keV deexcitation between the $X + 422.5$ keV level and the $I^\pi = 5^-$ ^{140m1}Eu.

$I^\pi = 6^-$ was found in Ref. [7] for the $X + 284.8$ keV level. It agrees with our measured value of $\alpha_K = 0.08(3)$ for the 284.8-keV line; we obtained it by gating on the 104.5-keV line, which indicates a mixed $M1 + E2$ multipolarity. It also establishes the sequence of the $M1 + E2$ 137.5-keV line deexciting the $X + 422.5$ keV 7^- level, and the 284.8-keV line feeding the ^{140m1}Eu isomer—opposite to the placement adopted in Ref. [6]. We place the observed 33.0-keV ($M1$) transition as deexciting the 7^- state at $X + 422.5$ keV to the new (7^-) level at $X + 389.2$ keV based on the transition intensity balance and consistency of the adopted transition multipolarities. The $E2$ multipolarity assignment for the 33.0-keV line would not allow for the observed γ-ray intensity.

The multipolarities listed for the transitions following ^{140m2}Eu decay in the decay scheme (see Fig. 8) offer a consistent picture of incoming and outgoing intensities for each intermediate level. Each cascade connecting the two isomeric states is consistent with the spin difference of 3 and opposite parities of the isomers.

The Weisskopf estimate for the partial half-lives of the 37.1- and 98.1-keV $E1$ transitions are 5 ps and 0.27 ps, respectively. The retardation factors are about 1.2×10^5 and 8.7×10^6, respectively.

Results from the neighboring odd-N even-Z nuclei, such as ^{139}Sm [25], suggest that the most important contribution for the negative-parity states comes from the $h_{11/2}$ neutron orbital where yrast bands are built on top of it. In the odd-Z even-N nuclei, such as ^{141}Eu [26,27], the proton is a decoupled $h_{11/2}$. Such a pattern of single-particle levels suggests for neighboring odd-Z odd-N nuclei the presence of the $\pi h_{11/2} \otimes \nu h_{11/2}$ and the $\pi h_{11/2} \otimes \nu s_{1/2}$ configurations at low energies. We interpret the ^{140m1}Eu metastable state as arising from the coupling of the $h_{11/2}$ proton to an $s_{1/2}$ neutron, with possible contribution of the $h_{11/2}$ proton coupled to the $d_{3/2}$ neutron, leading to an $I^\pi = 5^-$ state. The 1^+ ground state results from the $\pi d_{5/2}$ and $\nu d_{3/2}$ coupling. The $I^\pi = 5^-$ identified for the 125-ms isomeric state [1], the spin difference of 3, and parity change deduced for the transitions connecting the two isomers are consistent with the spin and parity of 8^+ for ^{140m2}Eu. The wave function of ^{140m2}Eu is likely to be dominated by the $\pi h_{11/2} \otimes \nu h_{11/2}$ component, as was also recognized in Refs. [6,7].

B. ^{142}Tb

Two isomeric levels were reported earlier for ^{142}Tb: 15(4)-μs ^{142m2}Tb at 620 keV [9,10] and 303-ms ^{142m1}Tb at 280 keV above the $I^\pi = 1^+$ ground state [1].

The data collected with the RMS optimized for $A/Q = 142/24$ recoils revealed γ lines of 178, 280, and 284 keV known to be transitions in ^{142}Eu [1]. The K-electron energies at 231 and 235 keV for the 280- and 284-keV transitions, respectively, were detected in the conversion electron spectrometer. The conversion coefficients of the 280- and 284-keV transitions were previously measured by Firestone *et al.* [1] in the study of the β decay of ^{142}Gd ($T_{1/2} = 70$ s). Using this information, we found that the effective BESCA efficiency was about 0.32% during the $A = 142$ measurement for the electron energies from about 50 keV to 1 MeV. The internal efficiency calibration of BESCA was used to verify the values of the conversion coefficients for transitions in ^{142}Tb by comparison of the relative intensities of K- and L-conversion electron lines.

The γ-ray spectrum resulting from the decay of ^{142m2}Tb, measured within a 90-μs time correlation window of the MCP recoil signals is shown in Fig. 10. It has considerably better statistics in comparison with the data presented in Refs. [9,10]. We obtained a half-life of 25(1) μs (see Fig. 11), from the decay pattern of the summed 137.7-, 165.4-, 219.4-, and 302.9-keV lines. Based on collected γ-ray spectra, new γ lines with a half-life of 25 μs were observed (see Fig. 10) in coincidence with the known transitions given in Ref. [10]. The new transitions have energies of 32.2, 81.5, 115.8, 197.6, 335.1, and 340.1 keV. Figure 12 shows the γ-ray transitions in coincidence with the 197.6-keV line along with the decay pattern of the 197.6-keV line. The γ-ray spectrum in coincidence with the 32.2-keV line is shown in Fig. 13(a), and Fig. 13(b) shows the γ-ray transitions in coincidence with the 302.9-keV line that represents the strongest line in ^{142m2}Tb. The low-energy lines at 24 and 27 keV shown in Fig. 13(b) might result from the fluorescence from indium material present next to the Ge crystal in the LOAX detector.

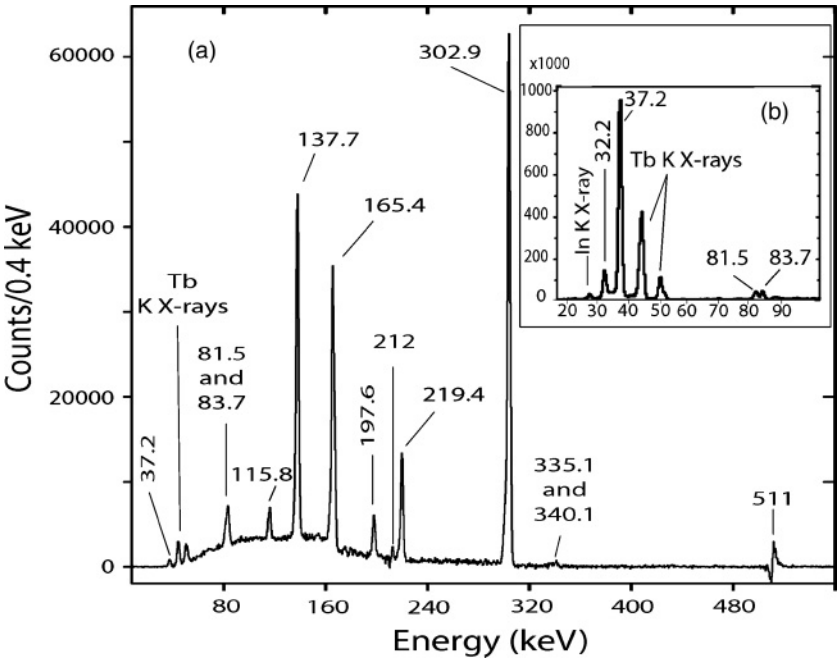

FIG. 10. Spectrum of γ rays measured by (a) two clover detectors and (b) LOAX detector appearing within 90 μs after implantation of mass 142 recoils.

The measured conversion electron spectra (see Fig. 14) allowed us to determine the multipolarities of several transitions. The experimental K/L ratios and the conversion coefficients given in Table II were used to establish multipolarities for the 137.7-, 165.4-, 197.6-, 219.4-, and 302.9-keV transitions deexciting ^{142m2}Tb. No electrons of energies below 85 keV or for very low-intensity γ-ray energies, such as the 335.1- and the 340.1-keV γ-ray transitions, were detected.

We extended the decay scheme of Ref. [10] for ^{142m2}Tb, as shown in Fig. 15. To account for the microsecond half-life of the isomer, none of the transitions depopulating ^{142m2}Tb can have a multipolarity higher than 2 as any γ ray with a multipolarity of 3 and higher will result in a Weisskopf partial half-life in the millisecond range and up to 2.1×10^{14} s for an $M4$ transition of the 32.2-keV line.

TABLE II. Relative intensities, K/L values, conversion coefficients, and transition multipolarities deduced for the isomeric decays in ^{142}Tb. The upper part represents the transitions deexciting the $\pi h_{11/2}\nu h_{11/2}$ ^{142m2}Tb, $T_{1/2} = 25\,\mu$s, $I^\pi = 8^+$. The lower part represents the transitions deexciting the $\pi h_{11/2}\nu s_{1/2}$ ^{142m1}Tb, $T_{1/2} = 303$ ms, $I^\pi = 5^-$.

E_γ	Rel. I_γ (%)		K/L	α_K or α_{total}	α_L	Adopted	I_{total}
(keV)	Present work	Literature[a]	(exp)	(exp)	(exp)	Multipolarity	(this work)
32.2(3)	13(1)	N/A		$\alpha_T = 14.6(76)$		$M1$	178(12)
37.2(3)	77(6)	81(25)		$\alpha_T = 1.5(5)$		$E1$	196(11)
81.5(3)	3(1)	N/A		$\alpha_T = 3.6(9)$		$M1$	15(3)
83.7(3)	3(1)	N/A		$\alpha_T = 6.3(27)$		$M1/E2$	15(3)
115.8(3)	3(1)	N/A			0.38(3)	$M1/E2$	5(1)
137.7(3)	38(3)	33(4)	5.1(2)	$\alpha_K = 0.53(1)$	0.10(2)	$M1/E2$	71(6)
165.4(3)	34(3)	34(4)	5.0(2)	$\alpha_K = 0.33(1)$	0.07(1)	$M1/E2$	51(7)
197.6(3)	5(1)	N/A	4.2(6)	$\alpha_K = 0.23(2)$	0.06(4)	$M1/E2$	7(1)
219.4(3)	13(1)	1(1)	3.7(4)	$\alpha_K = 0.14(1)$	0.04(1)	$M1/E2$	16(4)
302.9(3)	100(8)	100(7)	4.8(3)	$\alpha_K = 0.05(1)$	0.011(1)	$M1/E2$	108(9)
335.1(6)	1(1)	N/A				$E2$	1(1)
340.1(6)	1(1)	N/A				$M2$	4(1)
29.9(9)	<0.1	N/A				$M1/E2$	<48
68.2(3)	1.20(10)	N/A		$\alpha_T = 98^{+23}_{-10}$		$M2$	119^{30}_{16}
98.3(9)	<0.07	N/A		$\alpha_T < 180$	<2	$E3$	<3
181.8(3)	10(4)	6(2)	3.1(3)	$\alpha_K = 0.2(1)$	0.07(1)	$M1/E2$	14(6)
211.5(3)	100(6)	100(?)	2.6(1)	$\alpha_K = 0.11(1)$	0.04(1)	$E2$	199(13)

[a]The relative γ-ray intensities in the upper part of the table representing the γ-ray transitions in ^{142m2}Tb are from Ref. [10]. The relative γ-ray intensities in the lower part of the table representing ^{142m1}Tb are from Ref. [1].

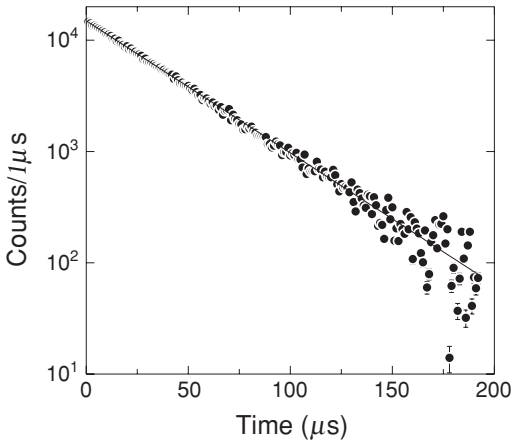

FIG. 11. Decay pattern of the sum of the 137.7-, 165.4-, 219.4-, and 302.9-keV γ-ray transitions after the appropriate background is subtracted. The fitted curve yields a half-life of 25(1) μs for ^{142m2}Tb.

From the transition intensity balance, the multipolarity of $M1, E1, M1$, and $M1 + E2$ was deduced for the 32.2-, 37.2-, 81.5-, and 83.7-keV lines, respectively. We deduced $\alpha_{\text{total}}(81.5\,\text{keV}) = 3.4(9)$ by comparing its intensity with that of the 137.7-, 165.4-, and 197.6-keV lines. This value of $\alpha_{\text{total}}(81.5\,\text{keV})$ is consistent with a mixed $M1 + E2$ character. We measured $\alpha_{\text{total}}(83.7\ \text{keV}) = 6.3 \pm 2.7$ by comparing its intensity with that of the 81.5-, 219.4-, and 115.8-keV lines. The α_{total} for the 83.7-keV transition is consistent with $E2$, but a $M1 + E2$ mixture cannot be ruled out. The $M1 + E2$ character of the 115.8-keV line fixes the spin and parity of the 395.6-keV level at 6^-. By comparing the intensity of the 32.2-keV line with that of the 302.9-, 165.4-, 83.7-, and 340.1-keV lines, we measure $\alpha_{\text{total}}(32.2\ \text{keV}) = 14.6 \pm 7.6$. This is consistent with an $M1$ multipolarity. The $M1$ character of the 32.2-keV lines allows for a spin and parity assignment of 6^- to the 311.9-keV level. The $I^\pi = 6^-$ of the 311.9- and 395.6-keV levels are consistent with the $M1 + E2$ character of the 83.7-keV line. Starting from the $I^\pi = 5^-$ level at

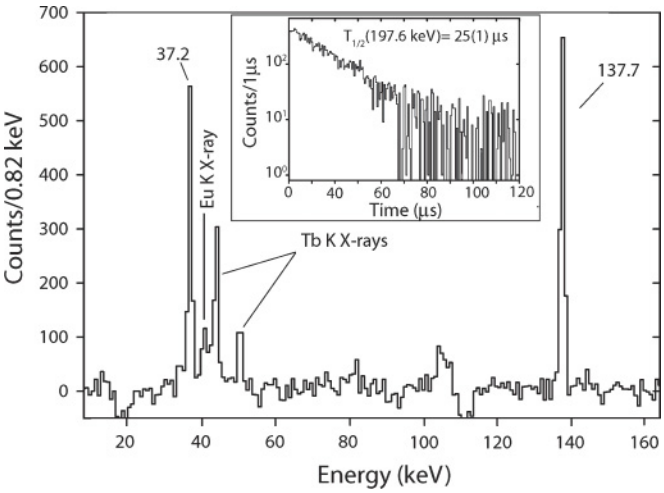

FIG. 12. The γ-ray spectrum in coincidence with the 197.6-keV line. Also shown is the decay pattern of the 197.6-keV line.

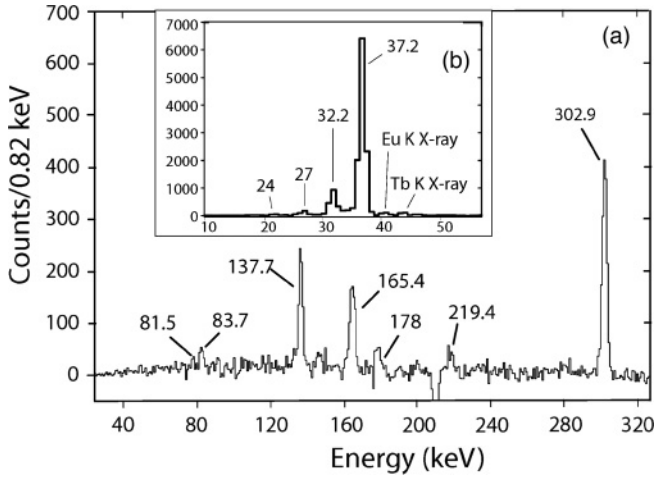

FIG. 13. The γ spectrum in coincidence with (a) the 32.2-keV line, and (b) the 302.9-keV line. The 24- and 27-keV lines are the In K x rays. The 178-keV line represents the strongest line in ^{142}Eu that contaminates our data.

279.7 keV, the sequence of $M1, M1 + E2$, and $E1$ for the 32.2-, 302.9-, and 37-keV lines, respectively, leads to an assignment of $I^\pi = 8^+$ for the $\pi h_{11/2} \otimes \nu h_{11/2}$ ^{142m2}Tb isomer. Weak γ lines at 335.1 and 340.1 keV, indicated by the dashed lines in Fig. 15, result at least partially from summing of stronger transitions with the 32.2- and 37.1-keV lines. The 340.1-keV line can have only the parity-changing $M2$ character whereas the 335.1-keV line can be assigned only the parity-conserving $E2$ character as shown in Fig. 15. The mixed multipolarities of $M1/E2$ observed for the 137.7, 165.4, and 302.9 keV lines agree with

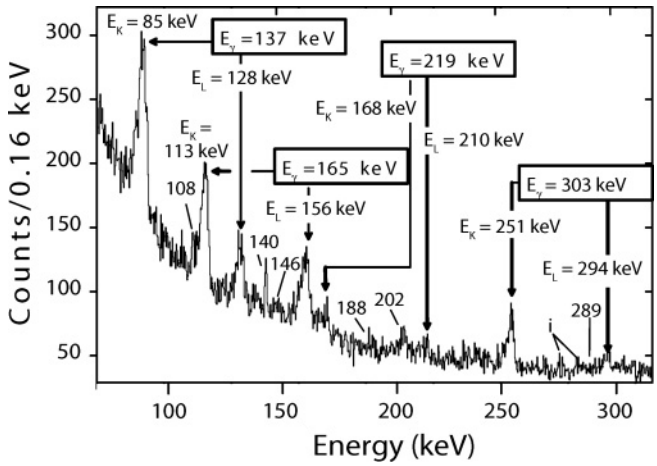

FIG. 14. Conversion electron data measured by the BESCA in the first 90 μs after the implantation of mass 142 recoils. The 108-keV line is the L-conversion lines for the 115.8-keV γ ray. The 146- and 188-keV lines are the K and L lines for the 197.6-keV γ-ray transition. The 140-keV line is just the 137.7-keV γ ray shifted by 2–3 channels. The 204-keV line is the L-conversion line for the 211.5-keV γ-ray. The lines labeled "i" are impurities from ^{142}Eu. They are the 273- and 277-keV L-conversion lines for the 280- and 284-keV γ-ray transitions in ^{142}Eu that are among the strongest lines in ^{142}Eu.

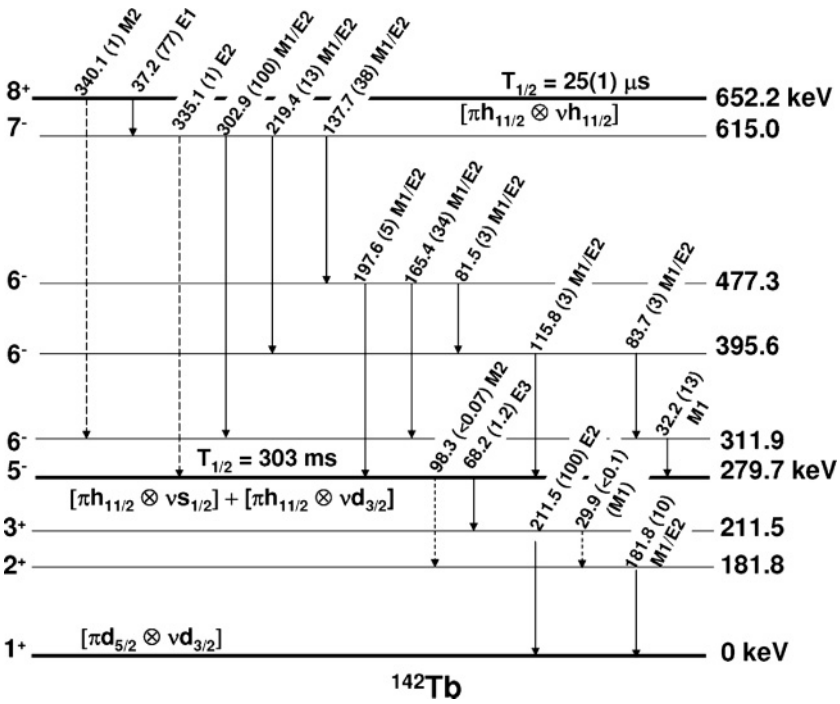

FIG. 15. ^{142}Tb level scheme.

the level scheme displayed in Fig. 15 and the decay properties listed in Table II.

The measurements of the properties of the transitions following the decay of the 303-ms isomer were more difficult. The useful range for recoil-decay correlations that discriminate long-lived activities was limited to a few milliseconds because of the implantation rate of about 200 pps. However, when the first 5-ms time gate was applied after implantation, the conversion electron lines corresponding to the decay of ^{142m1}Tb were clearly identified; see Fig. 16. The conversion coefficients for the 181.8- and 211.5-keV transitions in ^{142m1}Tb were determined from the conversion electron data measured by the BESCA and the γ-ray intensities of those transitions (see Table II). The measurements allowed us to assign the multipolarity $E2$ to the 211.5-keV transition whereas the 181.8-keV transition has mixed $M1/E2$ multipolarity. This points to a spin and parity of 3^+ and 2^+ for the levels at 211.5 and 181.8 keV, respectively, in agreement with Ref. [1]. The 68.2-keV line was observed in our LOAX and clovers spectrum. Its total intensity has to be at least equal to that of the 211.5-keV transition and should not be higher than the total intensity of both 211.5- and 181.8-keV transitions. The respective total conversion coefficient for the 68.2-keV line is therefore $\alpha_{\text{total}} = 98^{+23}_{-10}$, indicating an assignment of $M2$ multipolarity to this transition. This supports the $I^\pi = 5^-$ assignment for the 279.7-keV isomeric level in ^{142m1}Tb.

The presence of a 98.3-keV line in the decay scheme of ^{142m1}Tb [1] (see Fig. 15) is not clear. The γ-ray transition at 98.3 keV was not observed in our γ-ray spectrum; thus it must be strongly converted. Since the 181.8-keV level has an $I^\pi = 2^+$, the 98.3-keV line has to be an $E3$ to originate from $I^\pi = 5^-$ ^{142m1}Tb. The calculated α_{total} for the 98.3-keV $E3$ transition is 49 with an α_L contribution of 34. This means that, to account for the 181.8-keV line intensity, the 98.3-keV γ peak would have about 700–800 counts and the L electron conversion peak would be much stronger than the one shown in Fig. 16. Unfortunately, the K electron energy for the 98.3-keV γ ray in Tb is 46 keV. This is close to the energy of Eu K_β x rays that are emitted by ^{142}Eu produced in the β decay of ^{142}Gd ($T_{1/2} = 70$ s). Also, as mentioned above, no low-energy electrons were detected by the BESCA during our run. Measuring the number of counts at the energy of 98.3 keV in the LOAX spectrum gave us an upper limit of 920 counts. This is consistent with the calculated value of 760 counts for an $E3$ transition. A limit of $\alpha_{\text{total}}(98.3\text{ keV}) < 180$ could be derived assuming equal total intensities of 181.8- and 98.3-keV transitions. A 29.9-keV transition was suggested in Ref. [1]. In fact, a 29.9-keV $M1$ transition originating from the 211.5-keV $I^\pi = 2^+$ state could account for the intensity of the 181.8-keV transition as postulated in Ref. [1].

The relative intensities of the 68.2-, 181.8-, and 211.5-keV γ rays from the deexcitation of the ^{142m1}Tb isomer are listed in Table II.

The estimated Weiskopf partial half-life for the 37.2-keV $E1$ transition deexciting ^{142m2}Tb is 5 ps, whereas that of the 340.1 keV is 0.16 μs. A comparison with the experimental value indicates a retardation of about 1×10^7 for the half-life of the 37.2-keV transition.

C. ^{144}Ho

The 0.5-μs decay of the isomeric level and the excited levels built on this metastable state in ^{144}Ho were reported in Ref. [10]. We have observed four transitions, at 56.4, 59.9, 148.1, and 208.9 keV, listed in Ref. [10] as deexciting the ^{144m}Ho (see Fig. 17). The spectrum given in Fig. 17 results from gating measured γ energies by the first 1.5 μs of recoil-decay correlation time and subtracting the events obtained in correlation with the second 1.5-μs interval.

TABLE III. ^{144m}Ho [$T_{1/2} = 564(60)$ ns] γ transitions and intensities.

E_γ (keV)	Rel. I_γ (%)	Rel. I_γ (%) Ref. [9]	α_K, α_{total} (exp)	α_K, α_{total} (calc)	Adopted multipolarity	I_{total} (units)
40.2(3)	91(17)					
56.4(3)	100(17)	100(9)	$\alpha_{\text{total}} < 1.3$	$\alpha_{\text{total}} = 0.3(E1), 26.2(E2), 2.3(M1)$	$E1$	226(21)
59.9(9)	13(3)	11(1)	$\alpha_{\text{total}} = 12.6(46)$	$\alpha_{\text{total}} = 1.2(E1), 21.9(E1), 11.8(M1)$	$M1/E2$	176(76)
148.1(3)	99(18)	91(7)	$\alpha_K = 0.69(15)$	$\alpha_K = 0.09(E1), 0.39(E2), 0.73(M1)$	$M1/E2$	176(50)
208.9(3)	41(11)	54(6)		$\alpha_{\text{total}} = 0.05(E1), 0.21(E2), 0.34(M1)$	$E2$	50(13)

In addition, we observed a 40.2-keV line with a submicrosecond half-life correlated with the implantation of the $A = 144$ recoils; see Table III. The 40.2-keV line was observed in the spectrum measured by the low-energy LOAX detector (see Fig. 17), as well as in the spectrum recorded by the two clover detectors; compare Fig. 18. However, we were not able to place this transition in the ^{144}Ho level scheme because of low γ-γ coincidence statistics. Application of shorter or longer recoil γ correlation times did not reveal new activities.

We measured the half-life of ^{144m}Ho to be 564(60) ns (see Fig. 19), in agreement with the 500(20) ns given in Ref. [10].

We follow the level sequence in ^{144}Ho as proposed in Ref. [10], (see Fig. 20). By gating on the 59.9 keV line, we determined $\alpha_K(148.1\text{ keV}) = 0.69(15)$ by comparing the number of photons in the 148.1-keV γ ray to that of the Ho K_α x-ray. This value of α_K for the 148.1-keV line is consistent with an $M1 + E2$ multipolarity (see Table III). We were unable to accurately measure an α_K value for the 59.9 transition because of a lack of sufficient γ–γ counting statistics. However, a rough estimate of $\alpha_K(59.9\text{ keV}) = 14(5)$ was obtained from gating on the 148.1-keV line. The calculated $\alpha_K = 1.0, 2.3, 9.9$, and 122 for $E1$, $E2$, $M1$, and $M2$ multipolarities, respectively. With the large error bar, the measured α_K for the 59.9-keV line is consistent with a parity-conserving $M1 + E2$ transition character. By comparing the intensity of the 59.9-keV line with that of the 148.1-keV line we determined $\alpha_{\text{total}}(59.9\text{ keV}) = 12.6(46)$, which is also consistent with an $M1 + E2$ multipolarity (see Table III). The sequence of $M1/E2$ for the 59.9- and the 148.1-keV lines places a maximum spin and parity of $I^\pi = 7^-$ on the 208.9-keV level, which allows a multipolarity of $E2$ for the 208.9-keV γ transition with a calculated $\alpha_{\text{total}}(208.9\text{ keV}, E2) = 0.21$. With the $M1/E2$ and $E2$ characters for the 148.1- and 208.9-keV transitions, the measured $\alpha_{\text{total}}(56.4\text{ keV})$ has an upper limit of 1.26(43), which allows for only an $E1$ multipolarity (see Table III). The $E1$ character of the 56.4-keV line was also postulated in Ref. [10].

In Ref. [10], the quoted γ intensities for the 56.4-, 59.9-, and 148.1-keV lines are similar to our findings; see Table III. However, the $E1$ multipolarities adopted in Ref. [10] for the 56.1-, 59.9-, and 148.1-keV lines do not produce a consistent total intensity balance. In particular, the total intensities within the 148.1–59.9 cascade differ by a factor of ∼5 in Ref. [10]. The total intensity of the 56.4-keV transition cannot be reproduced by the sum of the 148.1- and 208.9-keV lines in Ref. [10]. Our measurements from the nieghboring odd-Z $N = 77$ isotones, namely ^{140m2}Eu and ^{142m2}Tb, indicate that all observed levels below the 0.5-μs isomer have negative parity. This fits to the $E2$ character of the 208.9-keV line as postulated in Ref. [10]. The transition intensity balance is consistent now; see Table III and Fig. 20.

The high-spin state $\pi h_{11/2} \otimes \nu h_{11/2}$ in ^{144}Ho is expected to be dominantly produced in the heavy-ion fusion-evaporation reaction, as suggested in Ref. [10]. Two transitions in ^{144m}Ho

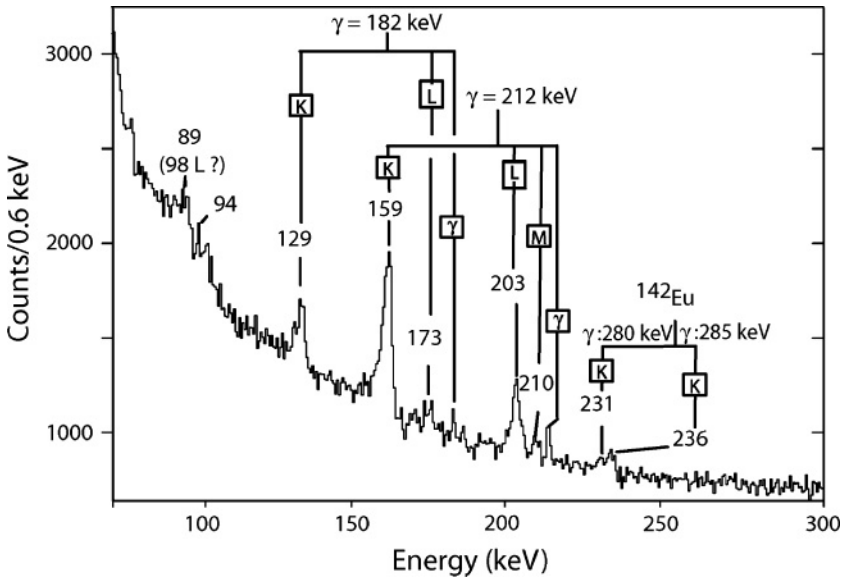

FIG. 16. Conversion electron data measured by the BESCA within the first 5 ms after a mass 142 recoil implantation.

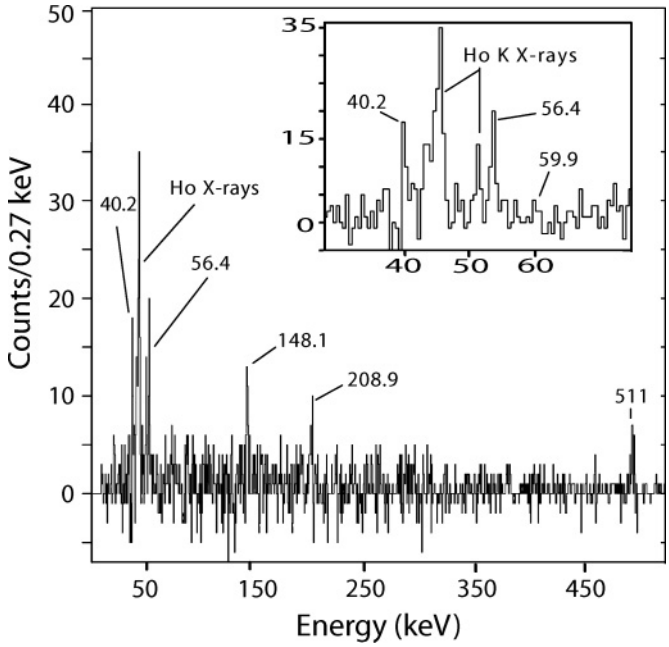

FIG. 17. γ spectrum associated with the decay of ^{144m}Ho measured by the LOAX detector within 1500 ns after implantation of mass $A = 144$ recoils. The upper panel shows the x-ray and low-energy γ-ray part of the spectrum.

decay, the 56.4-keV $E1$ and 208.9-keV $E2$, change the spin by up to three units and connect the high-spin state to the lowest observed state. The spin assignments of 8^+ for the high-spin isomer and 5^- for the the medium-spin state and also 9^+ and 6^- assignments are consistent with the isomeric decay properties. We adopt the 8^+ and 5^- sequence, as in the lower-mass $N = 77$ isotones, ^{140}Eu and ^{142}Tb. This suggests $I^\pi = 7^-$ and 6^- for the 208.9- and 59.9-keV levels, respectively (see Fig. 20). There was no experimental evidence obtained in our work or in Ref. [10] for a potential 1^+ ground state. A 1^+ ground state of ^{144}Ho can be expected from simple extrapolation of the level systematics of the neighboring lower-mass $N = 77$ isotones, ^{140}Eu and ^{142}Tb.

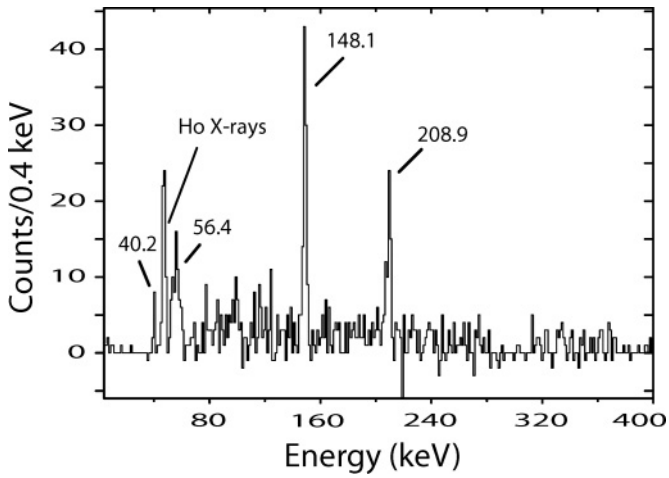

FIG. 18. γ spectrum measured by the clover detectors within 1500 ns after implantation of mass $A = 144$ recoils.

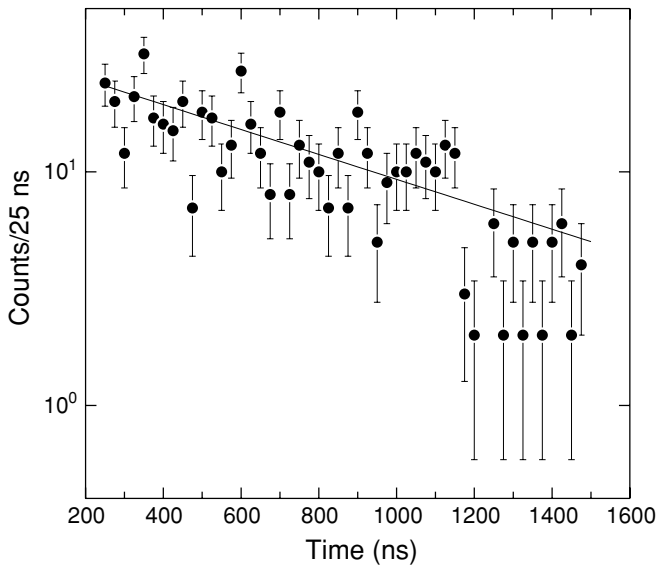

FIG. 19. Decay pattern of the sum of the 56.4-, 148.1-, and 208.9-keV γ rays in ^{144m}Ho after the appropriate background is subtracted. The fitted curve yields a half-life of 564(60) ns for ^{144m}Ho.

The observations in Ref. [10] and in this work might indicate that the 1^+ $[\pi d_{5/2} \otimes \nu d_{3/2}]$ configuration identified from the Gamow-Teller β-decay studies for ^{140}Eu and ^{142}Tb does not minimize the energy of higher-Z $N = 77$ even-mass isotones at the proton drip line. The proton orbital $d_{5/2}$ is filled for $Z = 67$ ^{144}Ho and a moderate-spin $(5^-, 6^-)$ $\pi h_{11/2} \otimes \nu s_{1/2}$ level might be already the ground-state configuration.

The estimated Weiskopf half-life for the 56.4-keV line deexciting ^{144m}Ho with an $E1$ transition is 1.5 ps. A comparison with an experimental value of 0.5 μs yields a retardation factor of about 1×10^6.

D. Proton radioactive ^{146}Tm

Proton emission from the odd-odd $N = 77$ isotone ^{146}Tm was first reported in Ref. [28], with two proton transitions observed. The measured energies and half-lives

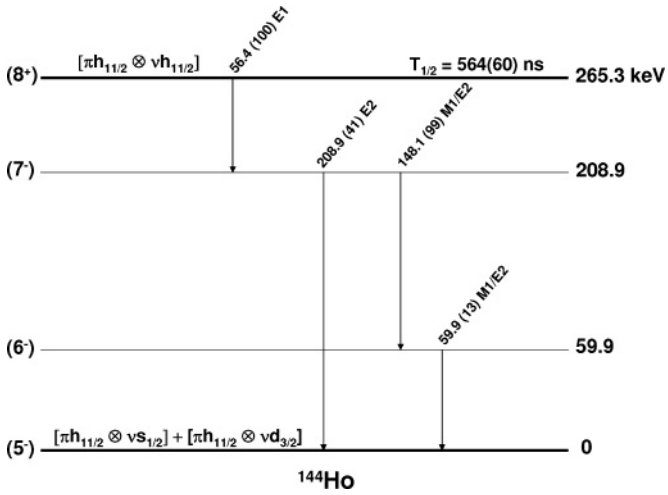

FIG. 20. ^{144}Ho level scheme.

were given as $E_p = 1.119(5)$ MeV and $T_{1/2} = 235(27)$ ms, $E_p = 1.189(5)$ MeV and $T_{1/2} = 72(23)$ ms, respectively. Reinvestigation of the ^{146}Tm activity at the HRIBF [2] resulted in the identification of three additional proton transitions, at 1.01 MeV, $T_{1/2} = 110(50)$ ms, at 0.94 MeV,$T_{1/2} = 80(30)$ ms, and at 0.89 MeV, $T_{1/2} = 190(50)$ ms. The decay patterns of the 1.120- and 1.191-MeV lines yielded more accurate half-lives of 200(10) and 80(10) ms [2], respectively.

Based on the similarity of the measured half-lives, the transitions at 1.120 MeV and 0.89 MeV were assigned to the decay of the predominately $\pi h_{11/2} \nu h_{11/2}$ isomeric state ^{146m}Tm at 180-keV excitation energy, while the decay of the mostly $\pi h_{11/2} \nu s_{1/2}$ ground state of ^{146}Tm was postulated to deexcite by the 1.191- and 0.94-MeV transitions [2]. The spin and parities of $I^\pi = (8^+)$ and $I^\pi = (5^-)$ were proposed [2] for ^{146m}Tm and ^{146gs}Tm, respectively. The assignment of the 1.016-MeV line to either state was ambiguous. Even a possibility of a third proton-emitting state, of $I^\pi = 1^+$, was considered, but this case was rejected because the lifetimes expected for the $l = 2$ or $l = 0$ proton transitions at 1.016 MeV are too short.

The wave-function components for ^{146m}Tm and for ^{146gs}Tm were calculated in Ref. [2] by use of a spherical approach, which was a simplification for this transitional nucleus. These ambiguities led us to the experimental and theoretical reinvestigation of proton emission from the states in ^{146}Tm.

In the present study, the acquired statistics of proton events exceeded those of the previous study [2] by a factor of ∼5. The mass spectrum recorded by the MCP at the focal plane of the RMS before the blockers were closed (compare Sec. II) is shown in Fig. 21. It indicates that $A = 146$ and $A = 147$ recoils were transmitted with the RMS setting optimized for the $A/Q = 146/27$ and $A/Q = 146/26$ recoils. The two-slit three-blocker system was used to permit the $A = 146$ recoils

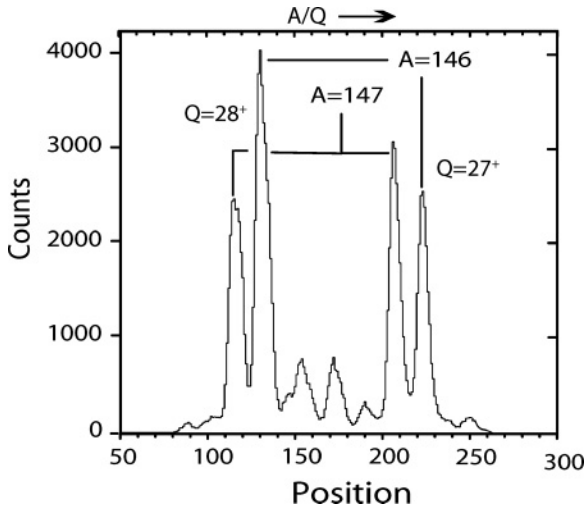

FIG. 21. Mass spectrum for the ^{146}Tm experiment measured by the large MCP detector at the focal plane of the RMS. The RMS was optimized for $A/Q = 146/27$ and $A/Q = 146/28$ recoils. A two-slit three-blocker system was used before the large MCP to allow $A = 146$ ions to reach the DSSD while stopping or reducing the implantation of other masses.

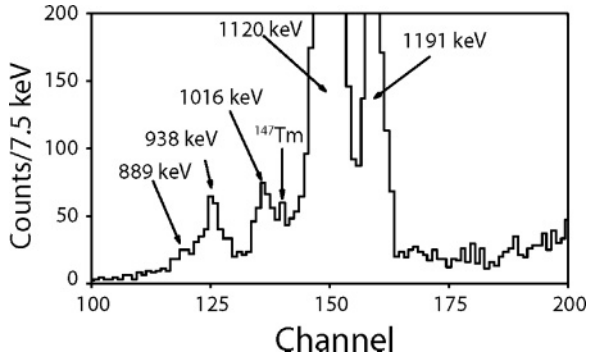

FIG. 22. Energy spectrum of protons correlated with implanted ^{146}Tm ions. The correlation time window for this spectrum was 200 ms. The spectrum was also gated by anticoincidence with the Sibox.

in both charge states to be implanted in the DSSD while eliminating the other masses. However, a small contamination of ^{147}Tm did appear in the DSSD proton spectra (see Fig. 22).

Improved statistics in the proton spectrum (see Fig. 22) allowed us to determine the half-lives of all five proton transitions with smaller uncertainty in comparison with the earlier work [2] (see Table IV). The half-life of each proton line was determined by fits to (1) the exponential decay of the time distribution of the events in the time interval 1–1200 ms, and (2) the growth of the integrated counts with time, as shown in Fig. 23. The data were fitted with the expression $C = C_0[1 - \exp(-\lambda_0 t)] + C_b[1 - \exp(-\lambda_b t)]$, where C_0 and C_b are the number of counts of the proton peak and the background, respectively, at infinity, and λ_0 and λ_b are the decay constants of the proton peak and the background, respectively. Both procedures of measuring the proton half-lives gave similar results.

On the basis of the measured half-life of 66(5) ms for the 1.016-MeV transition (see Fig. 23), we assign it to the 68-ms ground-state decay of ^{146}Tm (see Fig. 24). The half-life of the 0.89-MeV proton decay was determined to be 200(40) ms, as shown in Fig. 25. Thus the 0.89-MeV proton transition is assigned to the decay of 198 ms ^{146m}Tm, as in Ref. [2].

From a simple shell-model picture, one expects that ^{146}Tm would have five protons above the $Z = 64$ proton subshell, and five neutron holes below the $N = 82$ closed shell. The available single-particle orbitals for both protons and neutrons

TABLE IV. Proton energy (E_p) values, relative intensities, and half-lives ($T_{1/2}$) for the transitions observed in ^{146}Tm. The first three are assigned to the $I^\pi = 5^-$ ground state, while the last two originate from the $I^\pi = 10^+$ isomeric level.

E_p (keV)	Area[a]	I (%)	$T_{1/2}$ (ms)
938(4)	266(16)	20.0(13)	66(4)
1016(4)	357(19)	26.8(16)	66(5)
1191(1)	1333(39)	100(3)	68(2)
889(8)	100(40)	1.0(4)	200(40)
1120(1)	10393(102)	100(1)	198(3)

[a]Area was taken within the first 1200 ms after implant of $A = 146$ recoils

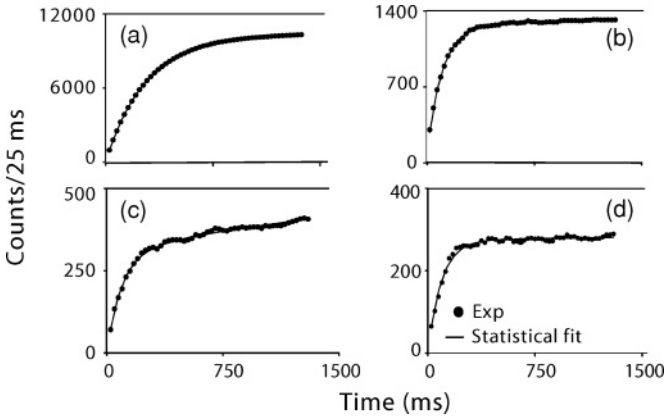

FIG. 23. Determination of the proton half-lives in ^{146}Tm decay by use of the exponential rise to maximum least-squares-fit function for the four proton energies: (a) 1.120 MeV, (b) 1.191 MeV, (c) 1.016 MeV, and (d) 0.938 MeV. The 1.016- and 0.938-MeV lines show bigger background components than the 1.120- and 1.191-MeV lines because of the close proximity of longer-lived lines, which are the 1.05-MeV line in ^{147}Tm and the 0.89-MeV line in ^{146m}Tm.

are therefore $h_{11/2}$, $s_{1/2}$, and $d_{3/2}$. These states, for both protons and neutrons, are known to be energetically very close, within a few hundred kilo-electron-volts, forming a subshell between proton (neutron) numbers 65 and 82. The $\nu s_{1/2}$ state minimizes the energy of the $N = 77$ even-Z isotones in this region (see Fig. 26).

The $\nu d_{3/2}$ and $\nu h_{11/2}$ single particle states above the $\nu s_{1/2}$ ground-state are shown in Fig. 26 together with the low-energy $I^\pi = 3/2^+$ and $5/2^+$ states of a $\nu s_{1/2} \otimes 2^+$ origin.

The $\pi h_{11/2}$ orbital was observed as a ground state for the neighboring thulium isotopes, ^{145}Tm [29,30] and ^{147}Tm [31]. The proton-emitting $\pi d_{3/2}$ states are known in ^{147}Tm and ^{151}Lu, at 60 keV [31] and 77 keV [32] above the $\pi h_{11/2}$ ground-state, respectively. The $\pi s_{1/2}$ states are known in heavier odd-mass Tm isotopes to be about 50 keV above the $\pi h_{11/2}$ orbital (see Fig. 3 in Ref. [32]).

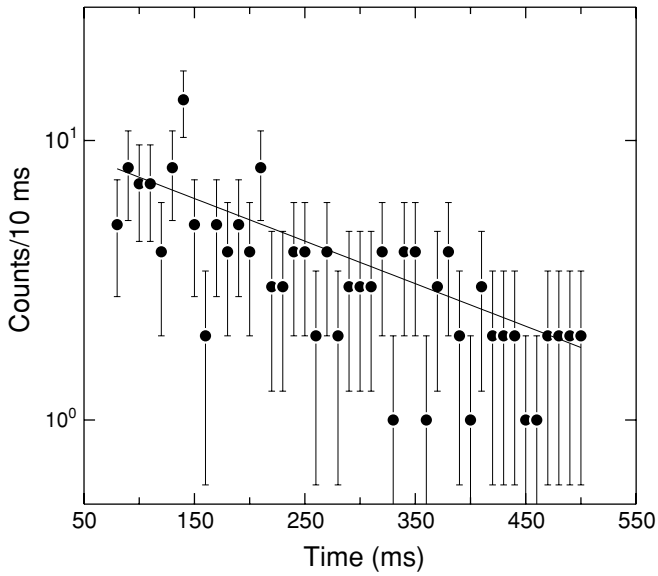

FIG. 25. Decay pattern of the 0.889-MeV proton line deexciting ^{146m}Tm after the appropriate background is subtracted. The fitted curve yields a half-life of 200(40) ms.

From the experimental level systematics of heavier odd-odd Tm isotopes and the odd-odd $N = 77$ isotones (see Fig. 1), one would expect an isomer with a spin and parity of 8^+ to 10^+, with a dominant configuration of $\pi h_{11/2} \otimes \nu h_{11/2}$, and a lower-spin state, possibly the ground state, of $I^\pi = 5^-$ or 6^- and main wave-function component $\pi h_{11/2} \otimes \nu s_{1/2}$ in ^{146}Tm. Both states can have a complex structure with admixtures contributing to their wave functions. For example, for the lower-spin state one can consider the mixing with the $\pi s_{1/2} \otimes \nu h_{11/2}$, $\pi d_{3/2} \otimes \nu h_{11/2}$, and $\pi h_{11/2} \otimes \nu d_{3/2}$ components, all coupled to the same spin of 5^- or 6^-. For both high-spin and medium-spin states, the $\pi h_{11/2}$ can be "substituted" by the $\pi f_{7/2}$ coupled to the 2^+ phonon representing the excited state of the ^{144}Er even-even core. Such a component in the

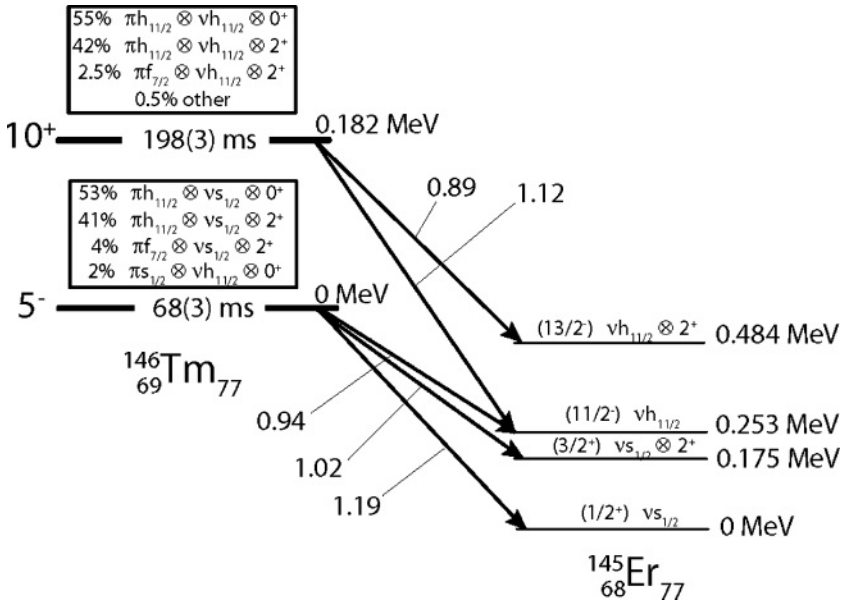

FIG. 24. The decay scheme of ^{146}Tm established in the present work.

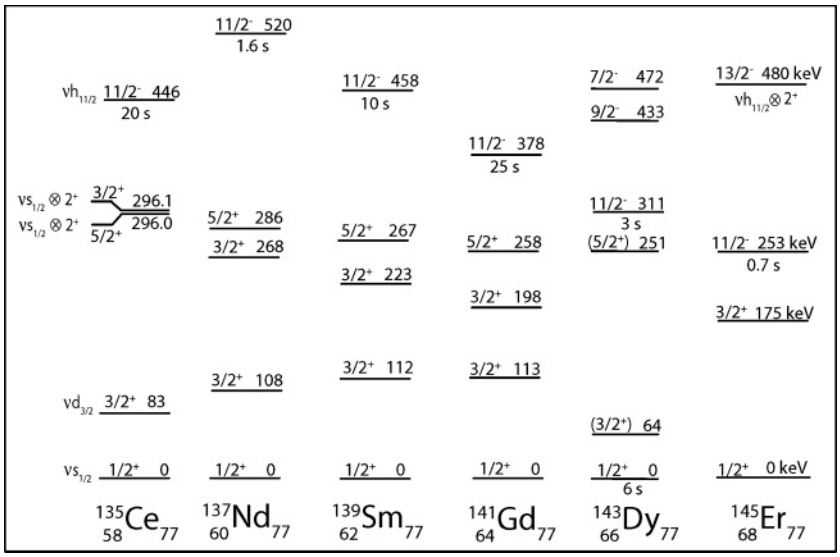

FIG. 26. Synopsis of the experimentally determined level systematics for the lightest $N = 77$ even-Z isotones. This figure is an extension of Fig. 1 from Ref. [2]. The level energies are labeled in kilo-electron-volts. The half-lives of the $\nu h_{11/2}$ isomeric states are also given.

wave function of ^{145}Tm explained the observed fine-structure line in its decay [30]. The 4% admixture of the $\pi f_{7/2} \otimes 2^+$ to the dominating $\pi h_{11/2}$ is responsible for the $I_p = 10\%$ proton transition from ^{145}Tm ($I^\pi = 11/2^-$) to the 2^+ first excited state at 0.33 MeV in ^{144}Er [30]. The analysis of the ^{145}Tm wave-function and proton-emission process was made within a particle-core vibration coupling model [30,33]. It accounted for the deformation of the ^{144}Er core, with $\beta_2 = 0.18$ deduced from the 0.33-MeV energy of the first 2^+ state [34,35]. This model was extended here to include coupling of the odd-neutron and is used here for the first time to interpret proton emission from an odd-odd nucleus, in our case ^{146}Tm.

1. High-spin ^{146m}Tm

We consider here the decay of the 198-ms level, populated much stronger in the fusion-evaporation reaction in comparison with the 68-ms activity. As in the earlier work [2], based on the similar half-life values of the 1.120- and 0.89-MeV proton transitions (see Table IV), we assume the same level of origin for these proton lines. New calculations also point to a large component of the wave function of ^{146m}Tm, the $\pi h_{11/2} \otimes 0^+ \otimes \nu h_{11/2}$, as responsible for the dominating $l = 5$, 1.120-MeV transition to the $\nu h_{11/2}$ bandhead in ^{145}Er, and to a smaller component, the $\pi f_{7/2} \otimes 2^+ \otimes \nu h_{11/2}$, as the origin of a weak $l = 3$, 0.89-MeV transition to an excited level built on the $\nu h_{11/2}$ bandhead. However, there is one major difference between our interpretation and that of Ref. [2]. As shown below, it is now clear that the isomer spin has to be at least 10^+, as in heavier odd-odd Tm isotopes rather than the (8^+) assignment that was suggested in Ref. [2]. It was overlooked in Ref. [2] that the coupling to the $I^\pi = 8^+$ state allows for the presence of the $\pi f_{7/2} \otimes 0^+ \otimes \nu h_{11/2}$ component in the ^{146m}Tm wave function that would trigger an $l = 3$, 1.120-MeV proton transition to the $\nu h_{11/2}$ bandhead, resulting in an approximately 50-ms partial half-life. Indeed, the particle-core vibration coupling model predicts a 1.7% contribution of such a configuration, if coupling to the $I^\pi = 8^+$ or even $I^\pi = 9^+$ state occurs. The branching ratio for the $l = 3$, 0.89-MeV line would then be much smaller, at the 0.01% level.

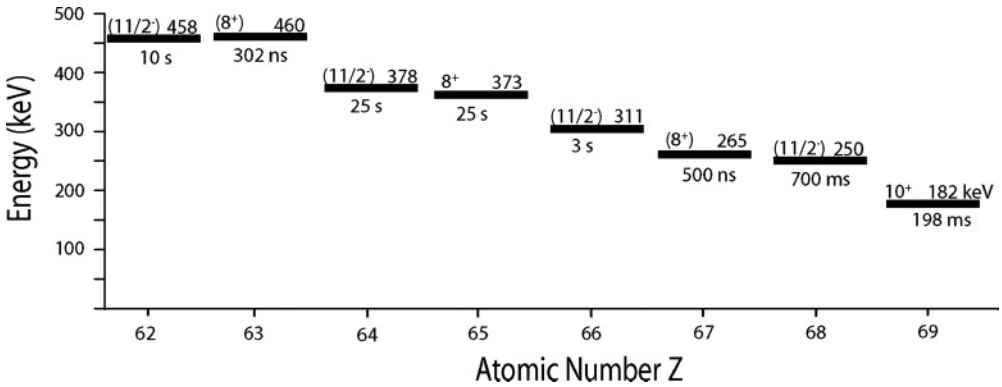

FIG. 27. Comparison of the energy differences between the $\pi h_{11/2} \nu s_{1/2}$ and $\pi h_{11/2} \nu h_{11/2}$ configurations with the energy difference of the $\nu s_{1/2}$ versus $\nu h_{11/2}$ configurations in the $N = 77$ isotones. The even-Z $N = 77$ isotones decay by means of β emission only while the odd-Z $N = 77$ isotones decay by means of γ-ray and particle emission.

TABLE V. Proton energy (E_p) values and branching ratios for the transitions observed in ^{146}Tm along with the wave functions of the two proton-decaying states. The first three are assigned to the $I^\pi = 5^-$, $T_{1/2} = 68(5)$ ms ground state, while the last two originate from the $I^\pi = 10^+$, $T_{1/2} = 198(3)$ ms isomer level.

E_p (keV)	Relative experimental proton branching ratio (%)	Wave function	Calculated contribution to the total width (%)	$\Delta\ell$	^{145}Er level energy (keV)
938	13.8(9)	2% $[\pi s_{1/2} \otimes 0^+] \otimes \nu h_{11/2}$	(15)[a]	0	253 ($11/2^-$)
1016	18.3(11)	4% $[\pi f_{7/2} \otimes 2^+] \otimes \nu s_{1/2}$	15	3	
		41% $[\pi h_{11/2} \otimes 2^+] \otimes \nu s_{1/2}$	0.003	5	175 ($3/2^+$)
1191	68.1(19)	53% $[\pi h_{11/2} \otimes 0^+] \otimes \nu s_{1/2}$	70	5	0 ($1/2^+$)
889	1.0(4)	2.5% $[\pi f_{7/2} \otimes 2^+] \otimes \nu h_{11/2}$	1.2	3	
		0.4% $\pi\ (\ell > 5) \otimes \nu h_{11/2}$			
		42% $[\pi h_{11/2} \otimes 2^+] \otimes \nu h_{11/2}$	0.04	5	484 ($13/2^-$)
1120	99(1)	55% $[\pi h_{11/2} \otimes 0^+] \otimes \nu h_{11/2}$	98.6	5	253 ($11/2^-$)
		0.1% $[\pi h_{9/2} \otimes 0^+] \otimes \nu h_{11/2}$	0.2	5	

[a]This value was inferred from experimental data but was not predicted by the particle-core vibration coupling model.

However, the coupling to the $I^\pi = 10^+$ (or to the $I^\pi = 11^+$) state excludes the $\pi f_{7/2} \otimes 0^+ \otimes \nu h_{11/2}$ component from the ^{146m}Tm wave function. The data on the half-life and fine-structure branching ratio of ^{146m}Tm do not really distinguish between the $I^\pi = 10^+$ or $I^\pi = 11^+$ state; compare Table 2 in Ref. [4], and see Table IV. However, since the $I^\pi = 10^+$ isomeric state was identified in ^{150}Tm [13] and suggested for neighboring ^{148}Tm [15], we follow such a spin assignment for ^{146m}Tm. It means that the 0.89-MeV $l = 3$ proton line should populate a negative-parity state, with a $\nu h_{11/2} \otimes 2^+$ configuration in ^{145}Er, with a spin equal to or higher than $13/2$. A recent in-beam study of the neighboring $N = 77$ isotone ^{143}Dy [36] shows a possible candidate for such a state at 122 keV above the $\nu h_{11/2}$ bandhead in a negative-parity band but with an unassigned spin value. The known 2^+ energy in ^{144}Er is 329(1) keV [30,37]. Therefore the energy difference of 230 keV between the $I^\pi = 11/2^-[\nu h_{11/2} \otimes 0^+]$ bandhead and the $I^\pi = 13/2^-[\nu h_{11/2} \otimes 2^+]$ state in ^{145}Er is reasonable. The calculated configuration and the proton-emission probabilities of the 10^+ isomer in ^{146}Tm are given in Table V.

Within the spherical approach discussed in Ref. [2], the wave function of the isomeric state was expected to be dominated by a 91% $\pi h_{11/2} \otimes \nu h_{11/2}$ configuration. The particle-core vibration coupling calculations show that 97% of the wave function contains the $\pi h_{11/2} \otimes \nu h_{11/2}$ component. However, this configuration is split into roughly equal parts by the coupling to the 0^+ and 2^+ states of the core; see Table V. This means that only about 55% of the wave function contributes to the $l = 5$ proton transition to the $\nu h_{11/2}$ bandhead in ^{145}Er. The remaining 42% of the $\pi h_{11/2} \otimes 2^+ \otimes \nu h_{11/2}$ component would add some negligible intensity to the $l = 5$ proton transition populating the $\nu h_{11/2} \otimes 2^+$ excited state.

2. *Medium-spin ^{146gs}Tm*

The short-lived 68-ms ^{146}Tm activity was assigned earlier [2] to the level resulting from the coupling of the $\pi h_{11/2}$ to the $\nu s_{1/2}$ nucleons. Since both orbitals are known to minimize the energy in the neighboring odd-mass nuclei, it is reasonable to expect that this proton-neutron state is the ground state of ^{146}Tm. The proton lines at 1.191 and 0.94 MeV were assigned to the decay of ^{146gs}Tm in Ref. [2]. From the similarity of the observed half-lives, we can now assign three observed proton transitions, at 1.191, 1.016, and 0.938 MeV, to the decay of the ground state. It was recognized earlier [28] that the intense 1.191-MeV proton transition has an $l = 5$ character, i.e., the proton originates from the $\pi h_{11/2}$ orbital. In Ref. [2] this proton line was interpreted for the first time as the ground-state to ground-state transition populating the $\nu s_{1/2}$ orbital in ^{145}Er. The particle-core vibration coupling model calculations indicate that the 1.016-MeV line originates from the 4% $\pi f_{7/2} \otimes 2^+ \otimes \nu s_{1/2}$ component of the wave function. The agreement between the observed and calculated decay probability is very good; see Table V. The $l = 3$, 1.016-MeV line populates the excited state at 182 keV in ^{145}Er associated with the $\nu s_{1/2} \otimes 2^+$ structure. A spin and parity of $3/2^+$ and $5/2^+$ are possible options. The low energy of 182 keV suggests the $3/2^+$ assignment based on the systematics shown in Fig. 26. If this is adopted, it means that the initial spin and parity of ^{146gs}Tm is $I^\pi = 5^-$ (the lowest spin populated by the $l = 3$ proton originating from $I^\pi = 6^-$ is $5/2^+$).

The 0.94-MeV line was identified in our previous work [2] as having $l = 0$ character resulting from a 4% "isospin-mirror" component in the ground-state wave function, the $\pi s_{1/2} \otimes 0^+ \otimes \nu h_{11/2}$. The calculated structure of the wave function, which now includes the $\pi f_{7/2} \otimes 2^+ \otimes \nu s_{1/2}$ part, requires about 2% of the isospin-mirror admixture to explain the relative intensities of the proton lines at 1.1911, 1.0166, and 0.938 MeV.

We have inspected theoretically the possibility of an $l = 3$ character for the 0.938-MeV transition feeding the $5/2^+$ level of the $\nu s_{1/2} \otimes 2^+$ configuration (instead of $l = 0$ feeding the $\nu h_{11/2}$ bandhead). The calculated intensity ratio of the 1.016- and 0.938-MeV transitions was 96:1, as one would expect for two proton transitions carrying the same orbital angular momentum l and having 80-keV energy difference. The observed intensities for the 1.016- and 0.938-MeV lines are similar to each other (see Table IV), which rules out this case.

The wave-function composition and decay width for both possible spin couplings, 5^- and 6^-, are listed in Table V.

3. Alternative decay pattern for ^{146}Tm

The assignment of the observed proton lines to only two decaying states in ^{146}Tm was made based on the similarity of the observed half-lives. Since the half-life uncertainties are relatively large for the weakest line at 0.89 MeV, one can at least consider the possibility for a third proton decaying state, below the discussed $I^\pi = 5^-$ state, with a half-life around 200 ms, but different from 198(3) ms. This possibility was suggested recently in Refs. [38,39] and supported by the recoil-decay tagging measurements, in which the γ-ray transitions correlated with the 1.120-MeV proton transition did not appear to be correlated with the weak 0.89-MeV transition.

The 1^+ ground state known in the odd-odd $N = 77$ isotones ^{140}Eu and ^{142}Tb was not observed for heavier ^{144}Ho (see Subsec. III C). These known 1^+ states were identified as the Gamow-Teller pairs [1] with $\pi d_{5/2} \otimes \nu d_{3/2}$ configurations. For heavier nuclei like ^{144}Ho and ^{146}Tm this state likely appears above the ground state since the $\pi h_{11/2}$ and $\nu s_{1/2}$ orbitals are closer to the Fermi surface than the respective d orbitals.

The $\pi d_{3/2} \otimes \nu s_{1/2}$ excited state in ^{146}Tm would decay by means of an $l = 2$ transition to the $\nu s_{1/2}$ ground state. Assuming a pure $\pi d_{3/2} \otimes \nu s_{1/2}$ configuration and accounting for the spectroscopic factor of the $d_{3/2}$ protons, one gets $\approx$400 ms for the partial half-life of the 0.89-MeV proton decay. The β decay contributing to the decay width of this state can reduce the half-life to the 200-ms level and make such a case feasible. However, as was pointed out above, the $\pi d_{3/2} \otimes \nu s_{1/2}$ configuration is unlikely to minimize the total energy of ^{146}Tm, so the proton transition from the $\pi d_{3/2} \otimes \nu s_{1/2}$ state to the $\nu s_{1/2}$ ground state of ^{146}Tm should have an energy greater than 1.191 MeV.

The ground state of ^{146}Tm is expected to be the point of change from prolate to oblate deformation, as was the case for the neighboring $N = 77$ odd-Z nuclei [40]. It is not obvious that such an effect can reduce the energy of the $\pi d_{3/2} \otimes \nu s_{1/2}$ configuration by 400 keV with respect to the $\pi h_{11/2} \otimes \nu s_{1/2}$ state and create the $\pi d_{3/2} \otimes \nu s_{1/2}$ ground state. However, it is an interesting problem worth further investigation. An in-beam study of the structure of ^{145}Er would be helpful to independently verify the properties of excited states populated by proton transitions. Also, to confirm the decay scheme of ^{146gs,m}Tm given in Fig. 24, it would be important to observe the γ transitions in prompt coincidence with the 0.89- and 1.016-MeV proton lines.

IV. SUMMARY

The systematics of the properties of metastable π-ν states in proton-rich odd-odd $N = 77$ isotones was established by use of decay spectroscopy methods. A 302-ns level in ^{140}Eu was found to be an $I^\pi = 8^+$ isomer arising from the coupling of the $h_{11/2}$ proton to the $h_{11/2}$ neutron. Its decay path terminates in the known $\pi h_{11/2} \otimes \nu s_{1/2}$ ^{140m1}Eu state. This sequence of metastable levels, with the ^{140m2}Eu state feeding the ^{140m1}Eu one, was determined experimentally. Most spin and parity values for the levels populated in the ^{140m2}Eu decay were firmly established, and we conclude that the isomer decays through retarded $E1$ transitions.

A half-life of 25(1) μs was measured for the decay of the high-spin isomer in ^{142}Tb, replacing the earlier reported value of 15(4) μs [9]. Spins and parities of 5^- and 8^+ for the isomeric levels in ^{142}Tb were unambiguously deduced from measured transition multipolarities. These states should have large components of the $\pi h_{11/2} \otimes \nu s_{1/2}$ and $\pi h_{11/2} \otimes \nu h_{11/2}$ configurations in their wave function, respectively. However, a respective isospin-mirror admixture, namely the $\nu h_{11/2} \otimes \pi s_{1/2}$ configuration, may also be present in the wave function of the medium-spin isomer, as indicated in Ref. [1]. New transitions were found to deexcite ^{142m2}Tb in this work, and the level scheme of ^{142m2}Tb was extended to account for these new transitions.

The decay scheme of the 0.5-μs ^{144m}Ho state given in Ref. [10] was consistent with our observations. The 59.9-, 148.1-, and 208.9-keV γ-ray transitions in ^{144m}Ho were found to have parity-conserving $M1 + E2$, $M1 + E2$, and $E2$ characters, respectively, opposite to the $E1$ multipolarity reported in Ref. [10].

The 1.016-MeV proton line, observed earlier [2] but not placed in the decay scheme of ^{146}Tm, was assigned to the decay of the shorter-lived ^{146gs}Tm with a half-life of 68(5) ms. This state is interpreted, within the particle-core vibration coupling model allowing for proton, neutron, and core coupling and accounting for the moderate deformation ($\beta_2 = 0.18$), as dominated by the $\pi h_{11/2} \otimes \nu s_{1/2}$ configuration coupled to the 0^+ and 2^+ states of the ^{144}Er core. The properties of proton emission do not distinguish between two possible spin couplings, to the $I^\pi = 5^-$ or 6^-. However, the state at 180 keV in ^{145}Er populated by the $l = 3$ proton transition from ^{146gs}Tm is more likely to be $3/2^+$ according to the level systematics, which supports the $I^\pi = 5^-$ assignment. The relative intensities of proton lines originating from the short-lived state are well reproduced within the particle-core vibration coupling model calculations. The calculated partial proton half-life of ^{146gs}Tm is about 79 ms, close to the measured value. This indicates that the decay width of this state is dominated by proton emission, with only about 14% contribution from β decay. The resulting partial half-life $T^\beta_{1/2}$ of 490 ms is of the order of 220 ms predicted for the β decay of ^{146}Tm [41].

The observed half-lives of ^{140m2}Eu, ^{142m2}Tb, and ^{144m}Ho indicate a strong hindrance of the $E1$ strength by a factor ranging from 10^5 to 10^7 with respect to the Weisskopf estimates. Large hindrances are in general typical for $E1$ transitions, but the transitions here may be additionally hindered by the differences in the structure of the initial and final levels. Different neutron orbitals, the $\nu h_{11/2}$ in the initial state and the $\nu s_{1/2}$ and $\nu d_{3/2}$ in the final state, contribute to the structure of the positive- and negative-parity levels in these odd-odd nuclei. One should note that direct γ decay between the neutron negative-parity $\nu h_{11/2}$ orbital and the states related to the positive-parity $\nu d_{3/2}$ and $\nu s_{1/2}$ orbitals does not occur in odd-mass $N = 77$ isotones near the proton drip line; see Fig. 27. These $\nu h_{11/2}$ states are known to decay by means of β transitions. The coupling of odd neutron particles to the $h_{11/2}$

proton facilitates the presence of strongly retarded $E1\gamma$-ray transitions connecting the positive-parity and negative-parity states; see Figs. 8, 15, and 20.

The ^{146m}Tm, $T_{1/2} = 198(3)$ ms, was assigned a spin and parity of $I^\pi = 10^+$, while the $I^\pi = (8)^+$ proposed earlier [2] is excluded by comparison with the particle-core vibration coupling model calculations. The wave function of ^{146m}Tm is dominated by the $\pi h_{11/2} \otimes \nu h_{11/2}$ component coupled to the 0^+ and 2^+ core states. A small 2.5% admixture of the $\pi f_{7/2} \otimes 2^+ \otimes \nu h_{11/2}$ configuration results in a branching ratio of 1.2% for the 0.89-MeV proton transition. This is close to the experimental value of ≈1%. The calculated partial proton half-life of the ^{146m}Tm is about 750 ms. As recognized earlier [2], the Gamow-Teller β decay, i.e., an allowed transformation of the $\pi h_{11/2}$ proton into a $\nu h_{9/2}$ neutron, governs the decay probability of ^{146m}Tm.

The observed sequence of levels in ^{144}Ho seems to resemble the basic properties of ^{146}Tm, with an apparent absence of the 1^+ ground state known for lower-mass $N = 77$ isotones. Also, a simple analysis of the energies of the single-particle orbitals near the Fermi surface in the ^{146}Tm region rather points to the existence of an excited 1^+ states. The 1^+ ground-state of ^{140}Eu and ^{142}Tb recognized earlier as the Gamow-Teller pair 1^+ $[\pi d_{5/2} \otimes \nu d_{3/2}]$ configuration [1] is likely to appear as an excited state in heavier $N = 77$ isotones since the $\pi h_{11/2}$ and $\nu s_{1/2}$ states are closer to the Fermi surface.

The evolution of the energy difference between the $\pi h_{11/2} \otimes \nu s_{1/2}$ and $\pi h_{11/2} \otimes \nu h_{11/2}$ configurations is given in Fig. 27 and shown to compare well with the $\nu h_{11/2}$ versus $\nu s_{1/2}$ energies in neighboring nuclei.

The decay of ^{146}Tm is an example of proton radioactivity study that contributes to the knowledge of neutron states in very exotic nuclei.

ACKNOWLEDGMENTS

Enlightning discussions with W.B.Walters are gratefully acknowledged. We extend thanks to the HRIBF staff for providing intense beams of ^{58}Ni and ^{54}Fe. The Joint Institute for Heavy Ion Research is supported by its members, University, of Tennessee, Vanderbilt University, and Oak Ridge National Laboratory. ORNL is managed by UT-Battelle, LLC, for the U.S. Department of Energy under contract no. DE-AC05-00OR22725. The work at the University of Tennessee in Knoxville, Vanderbilt University, Lousiana State University, Mississippi State University and UNIRIB was supported by the U.S. Department of Energy through grants and contracts no. DE-FG02-96ER40983, DE-FG05-88ER40407, DE-FG02-96ER40978, DE-FG02-96ER41006, DE-AC05-76OR00033. K. Rykaczewski was an Oak Ridge National Laboratory honor student.

[1] R. B. Firestone, J. Gilat, J. M. Nitschke, P. A. Wilmarth, and K. S. Vierinen, Phys. Rev. C **43**, 1066 (1991).
[2] T. N. Ginter *et al.*, Phys. Rev. C **68**, 034330 (2003).
[3] K. P. Rykaczewski *et al.*, AIP Conf. Proc. **764**, 223 (2005).
[4] J. C. Batchelder *et al.*, Eur. Phys. J. A **25**, s01, 149 (2005).
[5] K. P. Rykaczewski, Eur. Phys. J. A **15**, 81 (2002).
[6] D. M. Cullen *et al.*, Phys. Rev. C **66**, 034308 (2002).
[7] A. Hecht *et al.*, Phys. Rev. C **68**, 054310 (2003).
[8] P. A. Wilmarth *et al.*, Z. Phys. A **325**, 485 (1986).
[9] I. Zychor *et al.*, GSI Annual Report 1988, GSI 89-1, p. 31 (1989).
[10] C. Scholey *et al.*, Phys. Rev. C **63**, 034321 (2001).
[11] J. Gilat *et al.*, in *Proceedings of the Fifth International Conference on Nuclei Far From Stability*, Rousseau Lake, Ontario, Canada, 1987, edited by I. S. Towner, AIP Conf. Proc. No. 164, AIP, New York, p. 463 (1988).
[12] E. Nolte *et al.*, Z. Phys. A **306**, 223 (1982).
[13] R. Broda *et al.*, Z. Phys. A **334**, 11 (1989).
[14] A. Gadea *et al.*, Z. Phys. A **355**, 253 (1996).
[15] J. M. Nitschke, P. A. Wilmarth, J. Gilat, K. S. Toth, and F. T. Avignone III, Phys. Rev. C **37**, 2694 (1988).
[16] K. S. Toth, D. C. Sousa, J. M. Nitschke, and P. A. Wilmarth, Phys. Rev. C **35**, 620 (1987).
[17] C. J. Gross *et al.*, Nucl. Instrum. Methods A **450**, 12 (2000).
[18] D. Shapira *et al.*, Nucl. Instrum. Methods A **454**, 409 (2000).
[19] W. Królas *et al.*, Phys. Rev. C **65**, 031303(R) (2002).
[20] J. C. Batchelder *et al.*, Nucl. Instrum. Methods B **204**, 625 (2003).
[21] P. J. Sellin *et al.*, Nucl. Instrum. Methods Phys. Res. A **311**, 217 (1992).
[22] R. Grzywacz, Nucl. Instrum. Methods B **204**, 649 (2003).
[23] L. Westgard (ISOLDE Collaboration), Bull. Am. Phys. Soc. **17**, 907, CB13 (1972).
[24] R. Beraud *et al.*, in *Proceedings of the Third International Conference on Nucleus Nucleus Collision, Saint-Malo, France*, edited by Centre de Publications de L'Universitè de Caen, F-14032 Caen Cedex, France, p. 3 (1988).
[25] C. Rossi Alvarez *et al.*, Phys. Rev. C **54**, 57 (1996).
[26] J. Deslauriers *et al.*, Z. Phys. A **283**, 33 (1977).
[27] J. Gilat, J. M. Nitschke, P. A. Wilmarth, and R. B. Firestone, Phys. Rev. C **40**, 2249 (1989).
[28] K. Livingston *et al.*, Phys. Lett. **B312**, 46 (1993).
[29] J. C. Batchelder *et al.*, Phys. Rev. C **57**, R1042 (1998).
[30] M. Karny *et al.*, Phys. Rev. Lett. **90**, 012502 (2003).
[31] D. Seweryniak *et al.*, Phys. Rev. C **55**, R2137 (1997).
[32] C. R. Bingham *et al.*, Phys. Rev. C **59**, R2984 (1999).
[33] K. Hagino, Phys. Rev. C **64**, 041304(R) (2001).
[34] L. Grodzins, Phys. Lett. **2**, 88 (1962).
[35] S. Raman *et al.*, At. Data Nucl. Data Tables **78**, 1 (2001).
[36] J. R. B. Oliveira *et al.*, Phys. Rev. C **62**, 064301 (2000).
[37] D. Seweryniak *et al.*, Eur. Phys. J. A **25**, s01, 159 (2005).
[38] A. P. Robinson *et al.*, AIP Conf. Proc. **764**, 217 (2005).
[39] A. P. Robinson *et al.*, Eur. Phys. J. A **25**, s01, 155 (2005).
[40] P. Möller *et al.*, At. Data Nucl. Data Tables **59**, 185 (1995).
[41] P. Möller, R. Nix, and K.-L. Kratz, At. Data Nucl. Data Tables **66**, 131 (1997).